HHS Public Access

Author manuscript

Nature. Author manuscript; available in PMC 2023 December 14.

Published in final edited form as:

Nature. 2023 July ; 619(7970): 616–623. doi:10.1038/s41586-023-06256-5.

Reprogramming tumour-associated macrophages to outcompete cancer cells

Xian Zhang[1], **Shun Li**[1], **Isha Malik**[1], **Mytrang H. Do**[1,2], **Liangliang Ji**[1], **Chun Chou**[1], **Wei Shi**[1], **Kristelle J. Capistrano**[1], **Jing Zhang**[1], **Ting-Wei Hsu**[1,3], **Briana G. Nixon**[1,2], **Ke Xu**[1,2,#], **Xinxin Wang**[1,2], **Andrea Ballabio**[4,5,6,7], **Laura S. Schmidt**[8,9], **W. Marston Linehan**[8], **Ming O. Li**[1,2,*]

[1]Immunology Program, Sloan Kettering Institute, Memorial Sloan Kettering Cancer Center, New York, NY, USA 10065

[2]Immunology and Microbial Pathogenesis Program, Weill Cornell Graduate School of Medical Sciences, Cornell University, New York, NY, USA 10065

[3]Graduate Program in Biochemistry and Structural Biology, Cell and Developmental Biology, and Molecular Biology, Weill Cornell Graduate School of Medical Sciences, Cornell University, New York, NY, USA 10065

[4]Telethon Institute of Genetics and Medicine (TIGEM), Naples, Italy

[5]Medical Genetics Unit, Department of Medical and Translational Science, Federico II University, Naples, Italy

[6]Department of Molecular and Human Genetics, Baylor College of Medicine, Houston, TX, USA 77030

[7]Jan and Dan Duncan Neurological Research Institute, Texas Children's Hospital, Houston, TX, USA 77030

[8]Urologic Oncology Branch, National Cancer Institute, Bethesda, MD, USA 20892

[9]Basic Science Program, Frederick National Laboratory for Cancer Research, Frederick, MD, USA 21702

Summary paragraph

[*]Correspondence, lim@mskcc.org.

[#]Current affiliation, META Pharmaceuticals Inc., Shenzhen, China.

Author contributions

X.Z. and M.O.L. were involved in all aspects of this study, including planning and performing experiments, analysis and interpretation of data, and writing the manuscript. S.L. and X.Z. generated the *Fcgr1-cre* mice. I.M. assisted with mouse colony management. L.J. developed genotyping strategy for *Fcgr1-cre* mice. L.J., J.Z. assisted with mice dissection and tissue sample processing. M.H.D., L.J., C.C., W.S., K.J.C., J.Z., T.H., B.G.N., K.X. and X.W. assisted with mouse breeding, tumor measurement, and data analysis. L.S.S, W.M.L., and A.B. provided key mouse lines. All authors provided critical scientific feedback on results and manuscript.

Code Availability Code is available on request.

Competing interests

MSKCC has filed a patent application (number 63/502054) with the US Patent and Trademark Office directed towards targeting the nutrient-sensing pathway in macrophages for cancer immunotherapy. M.O.L. is a scientific advisory board member of and holds equity or stock options in Amberstone Biosciences and META Pharmaceuticals. A.B. is cofounder of Casma Therapeutics and advisory board member of Next Generation Diagnostics, Avilar Therapeutics and Coave Therapeutics. All other authors have no competing interests.

Metazoan organisms employ ‘cell competition’ as a cell quality control mechanism to eliminate unfit cells by their more robust neighbors[1,2], which could be maladapted to promote the selection of aggressive cancer cells[3–6]. As tumors are metabolically active and are populated by stroma cells[7,8], how environmental factors affect cancer cell competition remain elusive. Here, we show that tumor-associated macrophages (TAMs) can be dietarily or genetically reprogrammed to outcompete MYC-overexpressing cancer cells. In a murine model of breast cancer, MYC overexpression generated a mTORC1-dependent winner cancer cell state. A low protein diet inhibited cancer cell mTORC1 signaling and tumor growth, surprisingly due to the activation of transcription factors TFEB/TFE3 and mTORC1 in TAMs. Diet-derived cytosolic amino acids are sensed by Rag GTPases through GTPase activating proteins GATOR1 and FLCN to control Rag GTPase effectors including TFEB/TFE3[9–14]. Depletion of GATOR1 in TAMs suppressed TFEB/TFE3 and mTORC1 activation under the low protein diet condition, while depletion of FLCN or Rag GTPases activated TFEB/TFE3 and mTORC1 under the normal protein diet condition, causing accelerated or decelerated tumor growth, respectively. Furthermore, mTORC1 hyperactivation in both TAMs and cancer cells as well as their competitive fitness were dependent on the endolysosomal engulfment regulator PIKfyve. Thus, noncanonical engulfment-mediated Rag GTPase-independent mTORC1 signaling in TAMs controls TAM and cancer cell competition, which defines a novel innate immune tumor suppression pathway that may be targeted for cancer therapy.

The multistep process of carcinogenesis generates genetically heterogeneous malignant cells in dynamic interactions with the host organism; yet, the social rules that govern the communications among cancer cell variants, host cells, and other environmental factors have not been well characterized. High expression of the transcription factor MYC (also known as c-MYC) confers a ‘winner’ state in cell competition during development[15–18]. The *MYC* allele is frequently amplified in human malignancies[19–21], and MYC-high (MYC^{hi}) cancer cells are frequently adjacent to MYC-low (MYC^{lo}) dying cells in human malignancies[22], suggesting that MYC-mediated cell competition may define a mode of social cell behavior in tumor. Nonetheless, MYC overexpression alone is often insufficient to cause cell transformation and can instead trigger cell apoptosis[23,24]. How other oncogenic pathways promote the super-competitor status of MYC-overexpressing cancer cells and whether host factors regulate MYC-mediated cancer cell competition are poorly understood.

mTORC1 enables a MYC^{hi} winner cell state

MYC overexpression can be driven by *MYC* amplification, a highly prevalent genomic alteration in human malignancies including breast cancer (Extended Data Fig. 1a). Of note, *MYC* amplification, together with gain-of-function mutations of the *PIK3CA* gene encoding the p110a subunit of phosphoinositide 3-kinase, PI3K, can occur across molecular subtypes of human breast cancer and defined a group of breast cancer patients with the shortest relapse free survival (Fig. 1a, b, Extended Data Fig. 1b). To investigate MYC and PI3K cross-regulation in tumor development, we used a transgenic mouse model of breast cancer driven by the polyomavirus middle tumor antigen (PyMT) that activates PI3K[25]. PyMT mice were crossed with $Rosa26^{LSL\text{-}MYC}$ mice harboring a human *MYC* allele preceded with a *Loxp* site-flanked translational STOP sequence in the *Rosa26*

locus, and further onto the *S100a8-cre* transgenic background in which Cre recombinase is expressed in ~80% PyMT cancer cells[26]. Compared to control-PyMT mice, *S100a8-cre-Rosa26*$^{LSL\text{-}MYC/+}$PyMT (MYC-PyMT) mice exhibited earlier tumor onset and faster tumor growth (Fig. 1c). The accelerated tumor phenotype was associated with increased numbers of not only MYC^{hi} cancer cells but also apoptotic cancer cells defined by cleaved caspase 3 and cleaved PARP1 staining (Fig. 1d-f, Extended Data Fig. 1c, d). Notably, apoptotic cancer cells were MYC^{lo}, and were localized in close proximity to MYC^{hi} cancer cells (Fig. 1d, g, Extended Data Fig. 1c, e), suggesting that MYC-mediated cancer cell competition is induced in MYC-PyMT tumors.

MYC-mediated cell competition occurs in early mammalian embryos with MYC^{hi} winner epiblast cells exhibiting high anabolic activities[17]. The metabolic regulator mTORC1 has also been shown to arbitrate embryonic stem cell fitness selection[27]. MYC^{hi} winner cancer cells in MYC-PyMT mice were metabolically active with big cell sizes (Fig. 1d, Extended Data Fig. 1g), which was as well associated with mTORC1 hyperactivation marked by high level ribosomal protein S6 phosphorylation (p-S6^{hi}) and 4E-BP1 phosphorylation (p-4E-BP1^{hi}) (Fig. 1d, h, Extended Data Fig. 1c, f). To determine mTORC1 function in MYC-mediated cancer cell competition, we crossed *S100a8-cre-Rosa26*$^{LSL\text{-}MYC/+}$PyMT mice to the *Rptor*$^{fl/fl}$ background to deplete the mTORC1 scaffolding protein Raptor in cancer cells. In ~6 mm x 6 mm (length x width) tumors, Raptor deficiency corrected the cancer cell p-S6^{hi}, p-4E-BP1^{hi}, and size phenotypes in MYC-PyMT mice (Fig. 1d, h, Extended Data Fig. 1c, f), while cancer cell apoptosis was more prevalent (Fig. 1d, f, Extended Data Fig. 1c, d). Of note, in the absence of Raptor, MYC^{hi} cells were more readily to die than MYC^{lo} cells resulting in their depletion in tumors (Fig. 1d, e, g, Extended Data Fig. 1e). The altered cancer cell competition landscape resulted in attenuated tumor growth (Fig. 1c); yet, the tumor suppression phenotype was inferior to mice with Raptor depleted on the control-PyMT background (Fig. 1c). In later stage ~12 mm x 12 mm tumors from *S100a8-cre-Rosa26*$^{LSL\text{-}MYC/+}$*Rptor*$^{fl/fl}$PyMT mice, p-S6 was no longer suppressed, and MYC^{hi} cancer cells regained their winner status (Extended Data Fig. 1h-j), as a likely consequence of selection of cancer cells that had escaped biallelic *Rptor* deletion (Extended Data Fig. 1k-m). Together, these findings demonstrate an essential role for mTORC1 signaling to promote the competitive fitness of MYC^{hi} cancer cells in MYC-PyMT mice, and there is strong selection pressure for preserving mTORC1-active MYC^{hi} winner cancer cells in tumor aggression.

Discordant mTORC1 in cancer cell and TAM

To gain insights into how MYC and mTORC1 signaling regulate cancer cell competition, we performed RNA-sequencing experiments of control-PyMT and MYC-PyMT tumors. MYC-PyMT tumors manifested a gene expression program with higher expression of transcripts that support amino acid metabolism and aminoacyl tRNA biosynthesis, but lower expression of target genes that promote a cooperative cell behavior including those involved in focal adhesion and extracellular matrix receptor interaction, characteristics shared with human breast tumors with *MYC* amplification and *PIK3CA* gain-of-function mutations (Fig. 2a, Supplementary Table 1, Extended Data Fig. 2). Transcripts associated with cellular response to starvation were also enriched (Fig. 2a, Supplementary Table 1), implying that MYC-

PyMT cancer cells are under constant pressure to acquire nutrients such as amino acids to support protein synthesis. To investigate whether cancer cell competition might be regulated by the diet-derived amino acids, tumor burden-matched MYC-PyMT and control-PyMT mice were treated with an isocaloric low protein (LP) diet with 2% protein instead of the normal protein (NP) diet with 15% protein. Compared to the NP diet, the LP diet selectively inhibited tumor growth in MYC-PyMT, but not control-PyMT, mice (Fig. 2b).

Amino acids are not only building blocks for proteins, but also regulators of mTORC1 signaling in coordination with other cellular signals including PI3K[28,29]. Indeed, the attenuated tumor growth phenotype in the LP diet-treated MYC-PyMT mice was associated with diminished mTORC1 signaling in EpCAM-expressing cancer cells (Fig. 2c, d, Extended Data Fig. 3a, b). Surprisingly, while macrophages were depleted in MYC-PyMT tumors under the NP diet condition, a population of mTORC1-hyperactive macrophages were repopulated in the LP diet-treated MYC-PyMT tumors (Fig. 2c, e, f, Extended Data Fig. 3a, c). Previous studies have revealed two macrophage subsets in PyMT tumors: mammary tissue macrophages (MTMs) expressing the scavenger receptor MRC1 and TAMs expressing the cell adhesion molecule VCAM1, that contract and expand, respectively, during tumor progression[30,31]. Consistent with immunofluorescence assays, flow cytometry experiment revealed that the tumor parenchyma-localized TAMs were depleted in MYC-PyMT mice under the NP diet condition compared to control-PyMT mice, but repopulated under the LP diet condition, while the tumor stroma-localized MTMs or monocytes were unaffected (Fig. 2c, e, Extended Data Fig. 3d-f). In line with the mTORC1 hyperactivation phenotype, the repopulated TAMs in the LP diet-treated MYC-PyMT mice had bigger cell sizes (Fig. 2c, g, Extended Data Fig. 3e, g). Together, these findings reveal that NP and LP diets have opposing mTORC1 regulation functions in cancer cells versus TAMs in MYC-PyMT mice, and mTORC1 hyperactivation tracks with TAM growth and expansion.

TFEB/TFE3 drive TAM mTORC1 reprograming

To understand how the LP diet affected macrophage differentiation in MYC-PyMT tumors, we performed RNA-sequencing experiments of MTMs and TAMs isolated from the LP diet-treated control-PyMT and MYC-PyMT mice reconstituted with bone marrow cells from wild-type mice to eliminate potential leaky MYC expression in macrophages (Extended Data Fig. 4a-d). Consistent with phenotypic changes of TAMs but not MTMs between control-PyMT and MYC-PyMT tumors (Extended Data Fig. 3d-g), TAMs exhibited a higher degree of transcriptome variability than MTMs (Extended Data Fig. 4e, Supplementary Table 2). To further decipher how the LP diet regulated TAM differentiation in MYC-PyMT mice, we performed single-nucleus RNA-sequencing experiments as mRNA-sequencing could be contaminated with mRNA acquired from TAM engulfment of dying cells.
To fluorescently mark macrophage nuclei, we engineered a mouse strain with an expression cassette encoding tandem dimer Tomato (td-Tomato), T2A self-cleavage peptide and improved Cre (iCre) knocked into the 3' untranslated region of the *Fcgr1* locus (designated as *Fcgr1-cre*, Extended Data Fig. 5a, b). *Fcgr1-cre* mice were bred to the *Rosa26*$^{LSL\text{-}H2B\text{-}mCherry/+}$ background, which labeled macrophage nuclei with histone H2B fused to a monomeric Cherry fluorescent protein (H2B-mCherry) (Extended Data Fig. 5c, d). Control-PyMT and MYC-PyMT mice were reconstituted with bone marrow cells

from *Fcgr1-creRosa26*$^{LSL\text{-}H2B\text{-}mCherry/+}$ mice, subjected to the LP diet treatment, and followed by isolation of TAM nuclei for RNA-sequencing experiments (Extended Data Fig. 6a). Pooled data revealed three major clusters with MYC-PyMT TAMs preferentially distributed in cluster 3 (Extended Data Fig. 6b-d). Differential gene expression analyses showed that cluster 3 TAMs were enriched for transcripts encoding for proteins involved in phagolysosome biogenesis, phagocytosis, endocytosis, and cytoskeleton remodeling (Supplementary Table 3, Extended Data fig. 6e). In support of these observations, the lysosome marker LAMP1 was more highly expressed in TAMs from the LP diet-treated MYC-PyMT mice than control-PyMT mice (Extended Data Fig. 6f, g).

Expression of LAMP1 and other phagolysosome genes can be mediated by TFEB and TFE3 family of transcription factors[32,33]. Indeed, nuclear TFE3 was selectively detected in TAMs from tumors of the LP diet-treated MYC-PyMT, but not control-PyMT, mice (Fig. 3a, b). To determine TFEB and TFE3 functions in TAMs, bone marrow cells from *Fcgr1-cre-Tfeb*$^{fl/fl}$*Tfe3*$^{-/-}$ and control mice were used to reconstitute lethally irradiated MYC-PyMT mice that were further subjected to the LP diet treatment (Fig. 3c). Depletion of TFEB and TFE3 suppressed mTORC1 signaling in TAMs, and inhibited TAM growth and expansion in MYC-PyMT tumors (Fig. 3d-g, Extended Data Fig. 6h); surprisingly, mTORC1 signaling in cancer cells was enhanced, and the LP diet-induced tumor suppression was nullified (Fig. 3d, h, i,). Bone marrow cell reconstitution experiments were also performed with cells from *Fcgr1-cre-Rptor*$^{fl/fl}$ mice (Extended Data Fig. 6i). Raptor deficiency suppressed p-S6 signals in TAMs (Fig. 3j, k, Extended Data Fig. 6j), and additionally inhibited TAM growth and expansion (Fig. 3j, l, m), while MYC-PyMT cancer cell mTORC1 signaling and tumor growth were reinstated (Fig. 3j, n, o). These findings demonstrate that the loss of MYC-PyMT cancer cell mTORC1 signaling and winner cell status under the LP diet condition is non-cell-autonomous, but dependent on the gain of mTORC1 signaling in TAMs through TFEB and TFE3-dependent mechanisms.

Rag GTPases curtail TAM mTORC1 signaling

The transcription factor function of TFEB and TFE3 is regulated at the step of nuclear translocation with cytosol sequestration mediated primarily by binding to Rag family of small GTPases made of RagA or RagB in heterodimeric complexes with RagC or RagD[12–14,34]. Rag GTPases sense cytosolic amino acids in part through GATOR1 and FLCN that function as GTPase activating proteins for RagA/B and RagC/D, respectively[9,10]. Abundant cytosolic amino acids activate FLCN, and promote RagA/B in the GTP-bound state and RagC/D in the GDP-bound state (RagA/B^{GTP}-RagC/D^{GDP}) that recruits TFEB and TFE3 as well as mTORC1, while amino acid starvation activates GATOR1 and induces RagA/B^{GDP}-RagC/D^{GTP} that dissociates TFEB and TFE3 to promote their nuclear translocation[9–14,35] (Extended Data Fig. 7a). Notably, metabolic profiling experiments revealed that the levels of several amino acids including leucine that can be sensed by the Rag GTPase pathway[36–38] were reduced in the tumor interstitial fluid of the LP-diet-treated MYC-PyMT mice (Extended Data Fig. 7b, c, Supplementary Table 4). To determine whether the LP diet-induced TAM response acted through the Rag GTPase-mediated nutrient-sensing pathway, we generated *Fcgr1-cre-Depdc5*$^{fl/fl}$ mice to deplete the GATOR1 component Depdc5 in macrophages. Bone marrow cells from *Fcgr1-cre-Depdc5*$^{fl/fl}$ and

control mice were used to reconstitute lethally irradiated MYC-PyMT mice that were further subjected to the LP diet treatment (Extended Data Fig. 7d). Depdc5 deficiency abolished TFE3 nuclear translocation, and attenuated mTORC1 signaling in TAMs (Fig. 4a-c), in association with diminished TAM growth and expansion (Fig. 4a, d, e). Conversely, mTORC1 signaling was enhanced in cancer cells, and tumor growth was restored (Fig. 4a, f, g). These observations reveal that the LP diet is sensed through GATOR1 to activate TFEB and TFE3 as well as mTORC1 in TAMs, which is required to suppress mTORC1 signaling in MYC-PyMT cancer cells.

To determine whether gain of TFEB/TFE3-mTORC1 signaling in TAMs might be sufficient to restrain MYC-PyMT tumor development, we generated *Fcgr1-cre-Flcn*$^{fl/fl}$ mice to deplete FLCN in macrophages. Bone marrow cells from *Fcgr1-cre-Flcn*$^{fl/fl}$ and control mice were used to reconstitute lethally irradiated MYC-PyMT mice that were continuously fed with the NP diet (Extended Data Fig. 7e). Strikingly, depletion of FLCN led to TFE3 nuclear translocation and mTORC1 hyperactivation in TAMs promoting TAM growth and expansion (Fig. 4h-l, Extended data Fig. 7f), while cancer cell mTORC1 signaling and tumor growth were inhibited (Fig. 4h, m, n), essentially phenocopying MYC-PyMT mice fed with the LP diet (Fig. 2b-g). Bone marrow cell reconstitution experiments were also performed with cells from *Fcgr1-cre-Rraga*$^{fl/fl}$*Rragb*$^{fl/fl}$ mice to disrupt heterodimeric Rag GTPase complexes (Extended Data Fig. 7e, g, h), which largely recapitulated the phenotypes of mice reconstituted with *Fcgr1-cre-Flcn*$^{fl/fl}$ bone marrow cells (Fig. 4h-n). The Rag GTPase-mediated nutrient sensing pathway is essential for mTORC1 activation in some cell types including activated T lymphocytes *in vivo*[39,40]. Therefore, enhanced mTORC1 signaling in Rag GTPase-deficient TAMs is noteworthy, as it suggests that a crucial function for Rag GTPases is to inactivate TFEB and TFE3 in TAMs, in the absence of which, a noncanonical TFEB/TFE3-mTORC1 signaling pathway is induced to drive TAM reprograming in MYC-PyMT mice (Extended Data Fig. 7a).

Competing engulfment dictates fitness

Rag GTPases have been shown to suppress mTORC1 activation by the lysosome-derived amino acids acquired from macropinocytosis of extracellular proteins in cultured cell lines[41], raising the possibility that the LP diet-induced TAM mTORC1 signaling in MYC-PyMT mice might be driven by their scavenging proteinaceous materials in the tumor microenvironment including apoptotic cells and apoptotic bodies. In line with this hypothesis, TAMs isolated from the LP diet-conditioned MYC-PyMT tumors showed higher apoptotic cell-engulfing activities in a cell culture medium with lower amino acid levels (Extended Data Fig. 8a, b). Additionally, compared to the NP diet-treated MYC-PyMT mice, increased numbers of TUNEL-positive nuclei were observed in tumors from the LP diet-treated MYC-PyMT mice (Extended Data Fig. 8c, d), many of which were inside TAMs (Extended Data Fig. 8c, e). Bone marrow reconstitution experiments with donor cells from *Fcgr1-cre-Rosa26*$^{LSL\text{-}H2B\text{-}mCherry/+}$ mice to genetically label macrophage nuclei with H2B-mCherry showed that TUNEL-positive nuclei inside TAMs were not of macrophage origin (Extended Data Fig. 8f, g). As cancer cells from the LP diet-treated MYC-PyMT mice had low level mTORC1 signaling (Fig. 2d) and mTORC1 signaling supported the competitive fitness of MYC^{hi} cancer cells (Fig. 1d-h), we explored the possibility

that TUNEL-positive nuclei inside TAMs might be derived from apoptotic cancer cells. To this end, we reconstituted *S100a8cre-Rosa26*$^{LSL\text{-}MYC/LSL\text{-}H2B\text{-}mCherry}$PyMT mice with bone marrow cells from *H2B-EGFP* transgenic mice expressing histone H2B fused to an enhanced green florescent protein (Extended Data Fig. 9a), in which H2B-mCherry-positive nuclei inside H2B-EGFP-positive TAMs would mark TAM engulfment of cancer cells (Extended Data Fig. 9b). An average of three cancer cell nuclear particles were detected inside TAMs of the LP diet-treated MYC-PyMT tumors, while TAM engulfment events were rarely observed in the NP diet-treated MYC-PyMT mice (Fig. 5a).

To investigate whether engulfment was required for TAM reprograming and tumor suppression, we generated *Fcgr1-cre-Pikfyve*$^{fl/fl}$ mice to induce macrophage-specific depletion of PIKfyve, a lipid kinase required for lysosomal nutrient degradation and dissipation during phagocytosis, entosis, and macropinocytosis[42,43]. Bone marrow cells from *Fcgr1-cre-Pikfyve*$^{fl/fl}$ and control mice were used to reconstitute lethally irradiated *S100a8cre-Rosa26*$^{LSL\text{-}MYC/LSL\text{-}H2B\text{-}mCherry}$PyMT mice that were further subjected to dietary treatments (Extended Data Fig. 9c). In line with the finding that PIKfyve deficiency impairs macrophage engulfment actitivies[44,45], depletion of PIKfyve largely diminished the LP diet-induced TAM uptake of H2B-mCherry-labeled cancer cell nuclear particles (Fig. 5b, Extended Data Fig. 9d). In a separate bone marrow cell reconstitution experiment, PIKfyve deficiency attenuated TAM mTORC1 signaling in association with diminished TAM growth and expansion, while cancer cell mTORC1 signaling and tumor growth were regained in the LP diet-treated MYC-PyMT mice (Fig. 5c-h, Extended Data Fig. 9e). These findings reveal an essential role for the PIKfyve-mediated engulfment response in support of TAM mTORC1 activation, growth, and expansion as well as its tumor suppressor function.

Engulfment of loser cells by winner cells is required for tumor formation in a *Drosophila* model of epithelial cancer[46]. Cancer cell macropinocytosis of cell debris is also a critical route of nutrient acquisition to support cancer cell mTORC1 signaling and anabolism[47,48]. To investigate whether the restored cancer cell mTORC1 signaling in the LP diet-treated MYC-PyMT mice reconstituted with PIKfyve-deficient TAMs might be dependent on engulfment activities of cancer cells, bone marrow cells from *Fcgr1-cre-Pikfyve*$^{fl/fl}$ and control mice were used to reconstitute lethally irradiated *S100a8cre-Rosa26*$^{LSL\text{-}MYC/+}$ *Pikfyve*$^{fl/fl}$PyMT mice that were further subjected to the LP diet treatment (Extended Data Fig. 9e). PIKfyve-deficient cancer cells failed to activate mTORC1 triggered by depletion of PIKfyve in TAMs (Fig. 5c, g); nor was tumor growth enhanced (Fig. 5i). To further explore whether TAMs and cancer cells competed for the engulfment of bulky apoptotic cells and/or miniature apoptotic bodies, we labeled these dying cell materials with CellTrace Violet (CTV) and CellTrace Yellow (CTY) dyes, respectively, and co-injected them to MYC-PyMT tumors subjected to the LP diet treatment (Extended Data Fig. 9f). While both CTV and CTY signals were detected at high levels in TAMs, the CTY signal was more selectively present in cancer cells (Fig. 5j-n), in line with the observation that cancer cells more preferentially engulfed smaller apoptotic bodies in an *ex vivo* assay (Extended Data Fig. 9g, h). Notably, depletion of PIKfyve in TAMs impaired their engulfment of apoptotic cells and apoptotic bodies, and enhanced uptake of apoptotic bodies was selectively detected in cancer cells (Fig. 5j-n). Together, these findings demonstrate that TAM suppression of MYC-PyMT tumor growth is mediated by their

scavenger functions, which competes with cancer cells for engulfment-mediated nutrient acquisition and mTORC1 activation that acts as a shared fitness determinant for both TAMs and cancer cells (Extended Data Fig. 10).

Discussion

As an evolutionarily conserved cell fitness control mechanism, MYC-mediated cell competition has been implicated in tumorigenesis, but how it is induced and regulated are poorly defined due in part to the lack of mammalian models. Herein, in a murine breast cancer model driven by MYC and the PI3K activator PyMT, we found that MYC-mediated cell competition could be readily induced with mTORC1 fostering MYC^{hi} winner cancer cells for aggressive tumor growth. As a major metabolic regulator, mTORC1 senses a plethora of cell growth signals including amino acids that can be acquired via plasma membrane transporters or engulfment pathways[49]. A role for PIKfyve in support of cancer cell mTORC1 signaling underscores engulfment, and suggests that loser cancer cells may not perish in vain, but provide a nutrient source to support winner cancer cell aggression. Nonetheless, the exact extracellular cargo and cellular engulfment pathway that promote cancer cell mTORC1 signaling remain to be determined. Importantly, TAMs could be dietarily or genetically reprogramed to outcompete cancer cells for the engulfment-mediated nutrient acquisition and mTORC1 signaling in a process dependent on TFEB/TFE3 with TFEB/TFE3 activation suppressed by Rag GTPase sensing of a food source of amino acids. Yet, how TFEB/TFE3 drive Rag GTPase-independent mTORC1 signaling in TAMs is open for future investigation. The anti-tumor TAM reprogramming was induced in MYC-PyMT mice, but not in control-PyMT mice in which TAMs exert a pro-tumor immunosuppressive function[31,50]. Compared to control-PyMT cancer cells, MYC-PyMT cancer cells had diminished expression of transcripts that promote cell-to-cell and cell-tomatrix interactions, supporting a switch from cooperative to competitive modes of social interactions in the tumor tissue. Such a change of cancer cell behavior may fundamentally alter the differentiation trajectories and functional statuses of TAMs from cancer cell complicit to cancer cell competitor. Exploiting this distinct innate immune tumor suppression pathway holds promise for novel immunotherapy of aggressive malignancies triggered by cancer cell competition.

Methods

Mice

C57BL/6J, C57BL/6N-*Gt(ROSA)26Sor*$^{tm13(CAG-MYC,-CD2*)Rsky}$/J[51] (*Rosa26*$^{LSL-MYC}$, JAX stock #020458), B6.Cg-Tg(S100A8-cre-EGFP)1Ilw/J[52] (*S100A8-cre,* JAX stock #021614), B6.Cg-*Rptor*$^{tm1.1Dmsa}$/J[53] (*Rptor*^{fl}, JAX stock #013188), B6.Cg-*Pikfyve*$^{tm1.1Ashi}$/J[54] (*Pikfyve*^{fl}, JAX stock #029331), B6.Cg-Tg(HIST1H2BB/EGFP)1Pa/J[55] (*H2B-EGFP*, JAX stock #005418), and B6;129S-*Gt(ROSA)26Sor*$^{tm1.1Ksvo}$/J[56] (*Rosa26*$^{LSL-H2B-mCherry}$, JAX stock #023139) mice were purchased from the Jackson Laboratory. MMTV-PyMT, *Tfe3*$^{-}$, *Tfeb*^{fl}, *Flcn*^{fl}, *Rraga*^{fl}, and *Rragb*^{fl} mice were previously described[31,57–60]. *Depdc5*^{fl} mice were derived from mouse embryonic stem cells (ESCs) (*Depdc5*$^{tm1a(EUCOMM)Hmgu}$, EUCOMM) at Memorial Sloan Kettering Cancer Center (MSKCC) transgenic core facility

and crossed with *Rosa26*^{FLPe} mice[61] (JAX stock #003946) to remove the Neomycin resistance gene (NEO) cassette. *Fcgr1-cre* mice were generated by insertion of a targeting construct into the *Fcgr1* locus by CRISPR/Cas9-mediated homologous recombination in mouse ESCs on an albino C57BL/6 background. The targeting construct was generated by inserting between 2-kb homology arms upstream and downstream of the stop codon of the *Fcgr1* gene with IRES, tandem dimer (td) Tomato, T2A self-cleaving peptide, iCre recombinase and an FRT site-flanked PGK-NEO-BGHpA cassette. Double guide RNAs targeting at sites around the stop codon (5'-TTGTGCCCCAGTACTGTCAC-3') and (5'-CAAAGTTGACCCTGAAACTG-3') were cloned into the pX335 vector for a double nickase-targeting strategy. The targeting construct and pX335 vectors were co-injected into ESCs. Neomycin-resistant ESC clones were subject for Southern Blot analysis after BamHI restriction enzyme treatment to confirm proper insertion of the construct, and for karyotyping to confirm chromosome integrity. Clones with successful insertions and stable chromosomes were injected into pseudo-pregnant female C57BL/6 mice mixed with non-albino C57BL/6 ESCs. Of resulting pups, the construct successfully went germline, as noted by white fur chimerism and genotyped offspring. Mice harboring the targeted allele were subsequently crossed with *Rosa26*^{FLPe} mice to remove the NEO cassette. The *Fcgr1-cre* allele can be distinguished from the wild-type *Fcgr1* allele by PCR using the primer sets: Fcgr1-cre_Forward: 5'-GCGATGGCGTGTATGAAGAA-3', Fcgr1-cre_Reverse_1: 5'-AACATTCGACAACCCCCGC-3' and Fcgr1-cre_Reverse_2: 5'-CCGCCTTTGCAGGTGTATCTT-3'. All mice were back-crossed to the C57BL/6 background and maintained under specific pathogen-free conditions. In dietary switch experiment, irradiated isocaloric control (5CC7, TestDiet) and low protein (5BT9, TestDiet) diet chow were substituted for standard chow for mice with tumor burden around 250–350 mm^3. All animal experiments were conducted in accordance with procedures approved by the Institutional Animal Care and Use Committee of MSKCC.

Tumor measurement

Mammary tumors in female PyMT mice were measured weekly with a caliper. Tumor burden was calculated using the formula (L × W^2)/2, in which L is length and W is width. Total tumor burden was calculated by summing up individual tumor volumes of each mouse with an end-point defined when total burden reached 3,000 mm^3 or one tumor reached 2,000 mm^3.

Immunofluorescence of fixed frozen tissue

Tumors were collected from mice, washed with 1x PBS twice, fixed in periodate-lysine-paraformaldehyde for 16–24 h, dehydrated in 30% sucrose for 24 h, and then snap frozen in OCT. Tumor tissue in OCT was sectioned at 20 μm thickness, blocked for 60 min in staining buffer (0.1M Tris, 1% BSA, 1% FBS, 0.3% Triton X-100) and stained with fluorescently conjugated or unconjugated antibodies overnight at 4 °C. Slides were washed with 1x PBS and further stained for 1 h with fluorescently conjugated secondary antibody for unconjugated antibodies. Sequential staining using primary antibodies from same species were performed if necessary. Briefly, tissue stained with an unconjugated primary antibody was subsequently stained with a secondary antibody followed by staining with fluorescently conjugated primary antibodies raised from the same species. TUNEL assay was performed

using Click-iT Plus TUNEL Assay kit for *in situ* apoptosis detection with Alexa Fluor 488 dye (C10617, Invitrogen) according to the manufacturer's instruction before staining with fluorescently conjugated antibodies. All Slides were washed and counterstained with DAPI (4, 6-diamidino-2-phenylindole; Sigma), mounted with Fluoromount-G mounting solution (00–4958-02, Invitrogen), and dried in fridge overnight. Images were taken on several different models of microscopes, including confocal microscope LSM880 (Zeiss), SP5 (Leica) or widefield fluorescence microscope ZEN (Zeiss) using five- or four-color channels. Images were randomly captured from tumor tissues.

Cell isolation from tissues

Tumor-infiltrating immune cells were isolated from mammary tumors as previously described[12]. Briefly, tumor tissues were minced with a razor blade, followed by digestion in 350 U/mL Collagenase Type 3 (Worthington Biochemical) and 4 μg/mL DNase I (Sigma) in HBSS at 37 °C for 1 h with periodic vortex every 15 min. Digested tissues were passed through 100 μm filters and pelleted. To isolate immune cells, pellets were resuspended in 40% Percoll (Sigma) layered above 60% Percoll. Sample was centrifuged at 1,900 g at 4 °C for 30 min without brake. Cells at middle interface were collected, stained, and analyzed by flow cytometry or sorting. For cancer cells, cell pellets were resuspended in 40% Percoll and centrifuged at 1,900 g at 4 °C for 30 min without brake. Pelleted cells were collected, treated with red blood cell lysis buffer, washed with ice cold PBS, stained and analyzed by flow cytometry or cell sorting.

Flow cytometry and cell sorting

For flow cytometry experiments, cells were either pre-stained with blue fluorescence Live/Dead (Thermo Fisher Scientific) or post-stained with DAPI for the exclusion of dead cells. Cells were then incubated with 2.4G2 mAb to block FcγR binding, and panels of antibodies in 1x PBS containing 1.5% FBS and 2 mM EDTA for 30 min on ice. Intracellular staining of MRC1 was carried out using the Transcription Factor Staining Kit according to the manufacturer's manual (TONBO bioscience). All samples were acquired with an LSRII or Fortessa (BD), and analyzed with FlowJo software 10.5.x+ (Tree Star). Cell sorting was performed with a FACSAria II controlled by software FACSDiva (BD) using a 100 mm nozzle if not otherwise specified.

Single-nucleus RNA sequencing and data analysis

7-week-old control-PyMT and MYC-PyMT mice were lethally irradiated and reconstituted with 3 million total bone marrow cells from *Fcgr1-cre-Rosa26*$^{LSL\text{-}H2B\text{-}mCherry/+}$ mice as described previously[62]. Two weeks later, mice were switched to a low protein diet. 6-week post dietary switch, mice were sacrificed, and tumors were collected for immune cell isolation. TAMs were sorted based on their cell surface markers ($DAPI^{-}CD45^{+}SiglecF^{-}Ly6G^{-}B220^{-}Ly6C^{-}F4/80^{+}Vcam^{+}$). Nuclei were isolated with an EZ PREP kit (Sigma, Cat #NUC-101) according to the manufacturer's protocol, and intact nuclei without cell contamination were further sorted by fluorescent markers ($mCherry^{+}CD11b^{-}SYTO9^{+}$) for downstream processes. Following QC, the single nucleus suspension was loaded onto Chromium Chip B (10X Genomics PN 2000060) and GEM generation, cDNA synthesis, cDNA amplification, and library preparation proceeded using

the Chromium Single Cell 3' Reagent Kit v3 (10X Genomics PN 1000075) according to the manufacturer's protocol. cDNA amplification included 11 cycles, and 53–96 ng of the material was used to prepare sequencing libraries with 10–12 cycles of PCR. Indexed libraries were pooled equimolar and sequenced on a NovaSeq 6000 in a PE28/91 run using the NovaSeq 6000 SP or S1 Reagent Kit (100 cycles) (Illumina). An average of 30 thousand paired reads were generated per cell.

For single-nucleus RNA-sequencing analysis, FASTQ files were demultiplexed and transcriptome alignment to mm10 genome was performed using Cell Ranger 5.0. (10x genomics). Nuclei with greater than 0.5% mitochondrial gene expression were removed. Barcodes containing fewer than 10 or more than 20000 unique molecular identifiers (UMIs) were discarded. Normalization, clustering, and visualization were performed using Scanpy (v1.4.5). The clusters of nuclei with *Epcam* expression, that are remaining contaminated cancer cell nuclei, were further filtered out. The rest of the nucleus were visualized by TSNE plot. Significantly differentially expressed genes for each cluster were defined and computed for each cluster as genes differentially expressed in each cluster versus all others at adjusted $P < 0.05$ using Benjamii-Hochberg correction. For gene set analysis, significantly differentially expressed genes for each cluster were used as input. Adjusted P-values and enrichment ratio (overlapped/expected) against all KEGG pathway were calculated by WebGestaltR (v0.4.4) package with over-representation analysis using hypergeometric test. $-\text{Log}_2$(Enrichment ratio) were then plotted against $-\text{Log}_2$(adjusted P-value) for pathways enriched in cluster 3.

Bulk RNA sequencing and data analysis

For Extended Data Fig. 2, 6 mm x 6 mm tumors were collected from 15-week-old control-PyMT and MYC-PyMT mice, washed in 1x PBS twice, homogenized with mortar and pestle in liquid nitrogen, and resuspended in TRIZOL LS (Thermal fisher, 10296028) according to the total weight of tumors. For Extended Data Fig. 4c-e, 7-week-old control-PyMT and MYC-PyMT mice were lethally irradiated and reconstituted with 3 million total bone marrow cells from wild-type C57BL/6J mice, and treated with a low protein diet 2 weeks after. After 6 weeks of dietary switch, mice were sacrificed, and tumors were collected for immune cell isolation. TAMs ($DAPI^-CD45^+SiglecF^-Ly6G^-B220^-Ly6C^-F4/80^+Vcam^+$) and MTMs ($DAPI^-CD45^+SiglecF^-Ly6G^-B220^-Ly6C^-F4/80^+Vcam^-FOLR2^+$)[63] were sorted directly into TRIZOL LS reagents. RNA was extracted using the RNeasy Mini Kit (QIAGEN catalog # 74104) according to instructions provided by the manufacturer. RNA was eluted in 30 μL nuclease-free water. After RiboGreen quantification and quality control by Agilent BioAnalyzer, 500 ng of total RNA with RIN values of 3.3–9.6 underwent polyA selection and TruSeq library preparation according to instructions provided by Illumina (TruSeq Stranded mRNA LT Kit, catalog # RS-122–2102) with 8 cycles of PCR. Samples were barcoded and run on a HiSeq 4000 in a PE50 run, using the HiSeq 3000/4000 SBS Kit (Illumina). An average of 44 million paired reads were generated per sample. The percent of mRNA bases averaged 65%.

FASTQ files for bulk RNA-sequencing were first mapped to the mm10 genome using HiSat2 v2.0.542. The genomic index along with the list of splice sites and exons

were created by HiSat2 using the genome assembly GRCm38.p5 from ENSEMBL. Gene-level counts were computed using Rsubread. DESeq2 was used to perform differential expression analysis on the resulting count matrix. For RNA-sequencing experiment for control-PyMT and MYC-PyMT tumor tissues, genes significantly differentially expressed at adjusted $P < 0.05$ using Benjamini-Hochberg correction were shown in categories of amino acid synthesis, amino acid transporter, and ribonucleoproteins as heatmaps. For RNA-sequencing experiment for sorted TAMs and MTMs, principal component analysis (PCA) was performed on log transformed fold change of all differentially expressed genes using the prcomp package.

Human breast cancer data analysis

For Fig. 2a, breast cancer patient data were enrolled from METABRIC (Molecular Taxonomy of Breast Cancer International Consortium) breast cancer (BRCA) cohort (n = 2506). The relapse free survival analysis was conducted using log rank test in the subsets of patients with either hotspot driving mutations (based on significant occurrence) in *PIK3CA* (n = 388), *MYC* gene copy number amplification (n = 470), both (n = 83) or none (n = 1565) of these oncogenomic events. Gene set enrichment analysis (GSEA) was applied to differentially expressed genes (adjusted $P < 0.05$, student t-test with the Benjamini-Hochberg multiple comparison test correction) in the group of human patients with cooccurrence of *PIK3CA* mutation and *MYC* gene copy number amplification compared to all other groups with either single or no alteration in *PIK3CA* and *MYC*, and differentially expressed (adjusted $P < 0.05$, student t-test with the Benjamini-Hochberg multiple comparison test correction) genes between mouse control-PyMT and MYC-PyMT tumors, against WikiPathways, KEGG and REACTOME gene set databases. Significantly (FDR < 0.05 and $P < 0.05$) enriched gene sets overlapped between human and mouse data were plotted using both human and mouse normalized enrichment score (NES), with linear correlation calculated in Prism 9.x (GraphPad). Gene sets only significantly enriched in human or mouse dataset were also plotted with NES against NES = 0 for not significant species. Driver mutation of *PIK3CA* called from OncoKB, copy number alteration of *MYC* called from GISTIC 2.0, and gene expression data (z-score) were obtained from MSKCC's cBioPortal[64,65].

Tumor interstitial fluid extraction

Tumor-bearing control-PyMT and MYC-PyMT mice were treated with normal protein or low protein diets for 4 weeks, and the extraction was performed for one mouse at a time. After the mouse was euthanized, all ~6 mm x 6 mm tumors were dissected, washed in ice-cold PBS, dried with Kimwipes, and placed onto 40 μm cell strainer attached to 50 mL conical tube within 1 min. The tube was then centrifuged at 100 g at 4 °C for 15 min, and the supernatant of the flowthrough was carefully transferred to an Eppendorf tube and stored at −80 °C. Mice did not generate > 25 μl fluid were removed from the study due to not enough samples for subsequent processes.

NuGel-HemogloBind™ prep prior to metabolite extraction

Samples were removed from −80 °C storage to wet ice and thawed. Samples were brought through a NuGel-HemogloBind™ (Biotech Support Group) prep prior to extraction to

remedy the levels of hemolysis present. 20 μL of sample was added to a microfuge tube and mixed with 200 μL of HemogloBind Binding Buffer. Samples were then vortexed at room temperature for 3 min on a DVX-2500 Multi-Tube Vortexer (VWR International). The total volume (220 μL) was then transferred to a Spin-filter tube that was pre-conditioned with 50 mg NuGel-HemogloBind™ beads. The Spin-filter tubes were then vortexed again at room temperature for 10 min before centrifuging at 8000 g for 4 min.

Extraction of metabolites from tumor interstitial fluid

Extraction buffer, consisting of 82% methanol (Fisher Scientific), 1% Formic Acid (Millipore Sigma) and 512 nM metabolomics amino acid mix standard (Cambridge Isotope Laboratories, Inc.), was prepared and placed on dry ice. Samples were extracted by mixing 25 μL of sample with 975 μL of extraction buffer in 2 mL screw cap vials containing ~100 μL of disruption beads (Research Products International, Mount Prospect, IL). Each sample was homogenized for 10 cycles on a bead blaster homogenizer (Benchmark Scientific). Cycling consisted of a 30 sec homogenization time at 6 m/s followed by a 30 sec pause. Samples were subsequently spun at 21,000 g for 3 min at 4 °C. A set volume of each (450 μL) was transferred to a 1.5 mL tube and dried down by speedvac (Thermo Fisher). Samples were reconstituted in 50 μL of Optima LC/MS grade water (Fisher Scientific). Samples were sonicated for 2 min, then centrifuged at 21,000 g for 3 min at 4 °C. 20 μL were transferred to LC vials containing glass inserts for analysis. The remaining sample was placed in −80 °C for long term storage.

LC-MS/MS with the hybrid metabolomics

Samples were subjected to an LCMS analysis to detect and quantify known peaks. The LC column was a Millipore™ ZIC-pHILIC (2.1 × 150 mm, 5 μm) coupled to a Dionex Ultimate 3000™ system and the column oven temperature was set at 25 °C for the gradient elution. A flow rate of 100 μL/min was used with the following buffers: A) 10 mM ammonium carbonate in water, pH 9.0, and B) neat acetonitrile. The gradient profile was as follows: 80–20% B (0–30 min), 20–80% B (30–31 min), 80–80% B (31–42 min). Injection volume was set to 2 μL for all analyses (42 min total run time per injection). MS analyses were carried out by coupling the LC system to a Thermo Q Exactive HF™ mass spectrometer operating in heated electrospray ionization mode (HESI). Method duration was 30 min with a polarity switching data-dependent Top 5 method for both positive and negative modes. Spray voltage for both positive and negative modes was 3.5 kV and capillary temperature was set to 320 °C with a sheath gas rate of 35, aux gas of 10, and max spray current of 100 μA. The full MS scan for both polarities utilized 120,000 resolution with an AGC target of 3e6 and a maximum IT of 100 ms, and the scan range was from 67–1000 m/z. Tandem MS spectra for both positive and negative mode used a resolution of 15,000, AGC target of 1e5, maximum IT of 50 ms, isolation window of 0.4 m/z, isolation offset of 0.1 m/z, fixed first mass of 50 m/z, and 3-way multiplexed normalized collision energies (nCE) of 10, 35, 80. The minimum AGC target was 1e4 with an intensity threshold of 2e5. All data were acquired in profile mode.

Amino acid quantification

Amino acids were quantified in the interstitial fluid samples by taking the ratio to the respective double-labelled (13C/15N) amino acid standard (MSK-A2–1.2). The total moles of each amino acid internal standard added to the sample was calculated, and the dilution factor of the sample by the extraction buffer was taken into account to determine the concentration of sample amino acids before extraction. The resulting level was then multiplied by the dilution factor of the interstitial fluid before treatment with NuGel-HemogloBind to estimate the original interstitial fluid concentrations of amino acids.

Ex vivo and *in vivo* engulfment assay

A PyMT cell line derived from PyMT tumors was labeled with CellTrace Violet (CTV, ThermoFisher) or CellTrace Yellow (CTY, ThermoFisher) in PBS at 37 °C for 15 min in suspension, washed in PBS 2 times, and cultured at 37 °C in DMEM/F12 medium containing 50 μM H_2O_2 to induce apoptosis. Apoptotic cells were enriched from 8-h culture post apoptosis induction by centrifuge at 500 g for 3 min. Apoptotic bodies were enriched from 5-d culture post apoptosis induction by differential centrifugation at 500 g for 3 min and 20000 g for 10 min. For *ex vivo* engulfment assay, TAMs and cancer cells were isolated from mice of the indicated genotypes and diet treatment conditions, and seeded at 5×10^4 cells per well in the round bottom 96-well plate containing RPMI medium (2% FBS, amino acids reduced to 20% of RPMI). CTV-labeled apoptotic cells or apoptotic bodies generated from 2×10^5 cells were immediately added to the culture with brief centrifugation at 700 g for 3 min and incubated for 12 h. TAMs and cancer cells were then washed, stained with Fixable Viability Dye eFluor™ 780 (eBioscience), cell surface markers F4/80 and EpCAM, respectively, and subjected to flow cytometry analysis for CTV-positive cells. For *in vivo* engulfment assay, mice were pretreated with a low protein diet for 4 weeks. CTV-labeled apoptotic cells and CTY-labeled apoptotic bodies generated from 5×10^6 cells were prepared as described above, mixed in 50 μl HBSS buffer, and injected to 6 × 6 mm size tumors at multiple sites inside tumors using syringes attached to 33-gauge needles (Hamilton) in a slow pace to prevent leakage from the injection sites. After 8 h, mice were sacrificed, tumors were collected for TAM and cancer cell isolation and flow cytometry analysis of CTV and CTY signals.

Statistical analysis

All statistical measurements are displayed as mean ± S.D. P-values were calculated by an unpaired two-tailed Student's t-test for two-group comparisons, by one-way ANOVA for multi-group comparisons with the Tukey multiple comparison test correction, by two-way ANOVA for tumor growth curve comparisons, using Prims 9.x software (GraphPad).

Antibodies

The following antibodies were used in immunofluorescence assay: Anti-cleaved caspase 3 (Asp175, Cell Signaling, 1:100), anti-MYC (D84C12, Cell Signaling, 1:100), PE anti-phospho-S6 ribosomal protein (Ser240/244, D68F8, Cell Signaling, 1:100), anti-phospho-4E-BP1 (Thr37/46, 236B4, Cell Signaling, 1:50), Alexa fluor 594 anti-mouse EpCAM (G8.8, Biolegend, 1:300), Alexa fluor 647 anti-F4/80 (BM8, Biolegend, 1:200),

anti-TFE3 (HPA023881, Millipore Sigma, 1:50), Alexa fluor 488 anti-MRC1 (MR5D3, Bio-Rad, 1:200), anti-VCAM1 (AF643, R&D Systems, 1:100), APC anti-LAMP1 (1D4B, ThermoFisher, 1:100), Alexa fluor 647 goat anti-rabbit IgG (A21245, Invitrogen, 1:500), Alexa fluor 546 goat anti-rabbit IgG (A11035, Invitrogen, 1:500), Alexa fluor 488 goat anti-rabbit IgG (A11034, Invitrogen, 1:500), and Alexa fluor 546 donkey anti-goat IgG (A11056, Invitrogen, 1:500).

The following antibodies were used in flow cytometry analysis: BV650 anti-CD45 (30-F11, BD Biosciences, 1:300), eFluor 660 anti-Siglec-F (1RNM44N, eBioscience, 1:200), PE-Cy7 anti-B220 (RA3–6B2, Tonbo Bioscience, 1:200), PE-Cy7 anti-Ly6G (1A8, Tonbo Biosciences, 1:200), PE-CF594 anti-F4/80 (T45–2342, BD Biosciences, 1:200), APC-Cy7 anti-Ly6C (AL-21, BD Biosciences, 1:200), PerCP-Cy5.5 anti-MRC1 (C068C2, Biolegend, 1:200), PE and FITC anti-VCAM1 (429, eBioscience, 1:50), biotin anti-VCAM1 (429, BD Biosciences, 1:50), streptavidin PE (eBioscience, 1:500), PE anti-TCRβ (H57–597, Tonbo Biosciences, 1:200), PE-Cy7 anti-NK1.1 (PK136, Tonbo Biosciences, 1:200), APC-Cy7 anti-CD8α (53–6.7, Tonbo Biosciences, 1:200), BV510 anti-CD4 (RM4–5, BD Biosciences, 1:200), BV711 anti-CD11b (M1/70, BD Biosciences, 1:500), BV421 anti-CD11c (N418, BD Biosciences, 1:200), BV605 anti-MHCII (M5/114.15.2, BD Biosciences, 1:500), BV510 anti-XCR1 (ZET, Biolegend, 1:200), FITC anti-F4/80 (BM8.1, Tonbo Biosciences, 1:200), and APC anti-Folate receptor beta (94b/FOLR2, Biolegend, 1:200).

RT-qPCR primers

cre: Forward 5’-CGATGCAACGAGTGATGAGG-3’ and reverse 5’-CGCGCGCCTGAAGATATAGA-3’; *MYC*: Forward 5’-GGAACGAGCTAAAACGGAGC-3’ and reverse 5’-TTTGCTCCTCTGCTTGGACG-3’; *Rptor*: Forward 5’-CTGGCCTCATCGTCAAGTCC-3’ and reverse 5’-TTCATTGAGGGAGGCAAGGG-3’; *Pikfyve*: Forward 5’-CTTCGAAGCCTCAGCACAGT-3’ and reverse 5’-TGGTGTCTGCGCCTAAATGT-3’; *Flcn*: Forward 5’-GATGAACACTGCCTTCACGC-3’ and reverse 5’-GAGCTTTTCTGTCAGCCTGC-3’; *Tfeb*: Forward 5’-TGACAACATTATGCGCCTGG-3’ and reverse 5’-CTGTACACGTTCAGGTGGCT-3’; *Rraga*: Forward 5’-CTGCCTGGTGCACAAAATGG-3’ and reverse 5’-TGGACGTTCGAAAACAAGCG-3’; *Rragb*: Forward 5’-AATGTGGGCCCAAAAGTGGA-3’ and reverse 5’-AAGACGACGTGTGTCTCTGG-3’.

Extended Data

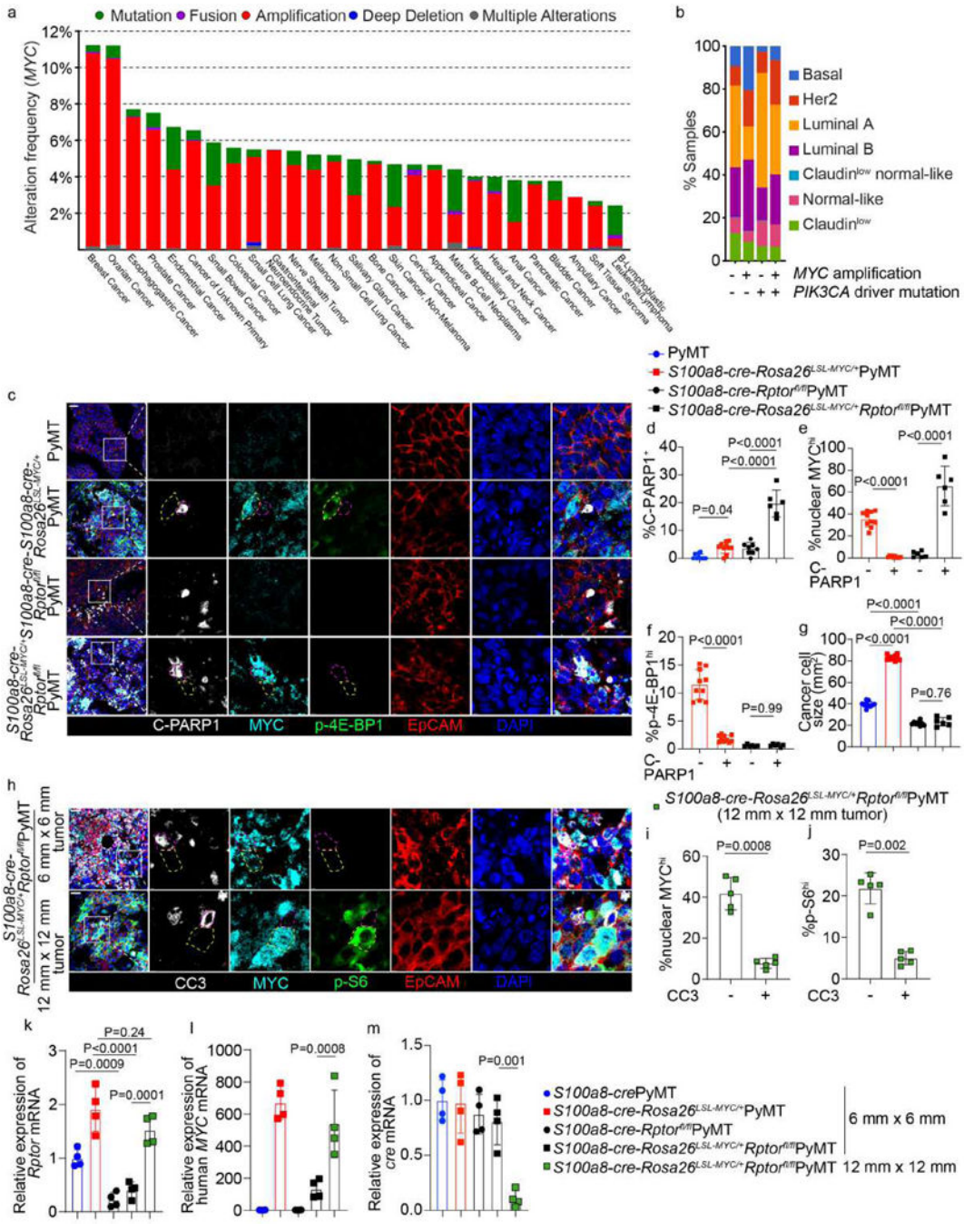

Extended data fig. 1. mTORC1 signaling supports the MYC-driven 'winner' status of cancer cells.

a, Frequency of *MYC* amplification across human malignancies with breast cancer being the most prevalent cancer type. **b**, Pam50 molecular subtypes in groups of human breast cancer samples with none, either or both of MYC amplification and PIK3CA driver mutation. **c**, Immunofluorescence images showing expression of cleaved PARP1 (C-PARP1), MYC, phosphorylated 4E-BP1 (p-4E-BP1), and EpCAM in 6 mm x 6 mm tumor tissue samples

from mice of the indicated genotypes. Scale bar: 20 μm. Representative 'loser' cells marked by magenta dashed lines and 'winner' cells marked by yellow dashed lines. **e, f**, Quantification of percentage of C-PARP1-positive cancer cells **(d)**, percentage of cells with high nuclear MYC expression or high p-4E-BP1 expression among C-PARP1-positive or −negative cancer cells from PyMT (n = 10), *S100a8-cre-Rosa26*$^{LSL\text{-}MYC/+}$PyMT (n = 10), *S100a8-cre-Rptor*$^{fl/fl}$PyMT (n = 8) and *S100a8-cre-Rosa26*$^{LSL\text{-}MYC/+}$*Rptor*$^{fl/fl}$PyMT (n = 6) tumors (**e, f**), and cancer cell size for tissue sections in Fig. 1d (**g**). **h**, Immunofluorescence images showing expression of cleaved caspase 3 (CC3), MYC, phosphorylated S6 ribosomal protein at serine 240/244 (p-S6), and EpCAM in 6 mm x 6 mm or 12 mm x 12 mm tumor tissue samples from *S100a8-cre-Rosa26*$^{LSL\text{-}MYC/+}$*Rptor*$^{fl/fl}$PyMT mice. Scale bar: 20 μm. Representative 'loser' cells marked by magenta dashed lines and 'winner' cells marked by yellow dashed lines. **i, j**, Quantification of percentage of cells with high MYC expression or high p-S6 expression among CC3-positive or −negative EpCAM-expressing cancer cells from *S100a8-cre-Rosa26*$^{LSL\text{-}MYC/+}$*Rptor*$^{fl/fl}$PyMT mice (n = 5). **k-m**, RT-qPCR analysis of *Rptor*, human *MYC*, and *cre* mRNA expression in cancer cells isolated from tumors of the indicated genotypes and tumor size (n = 4 mice for each group). All statistical data are shown as mean ± S.D. One-way ANOVA with the Tukey multiple comparison test correction in (**d-g, k-m**), and Two-sided Student t-test in (**i, j**).

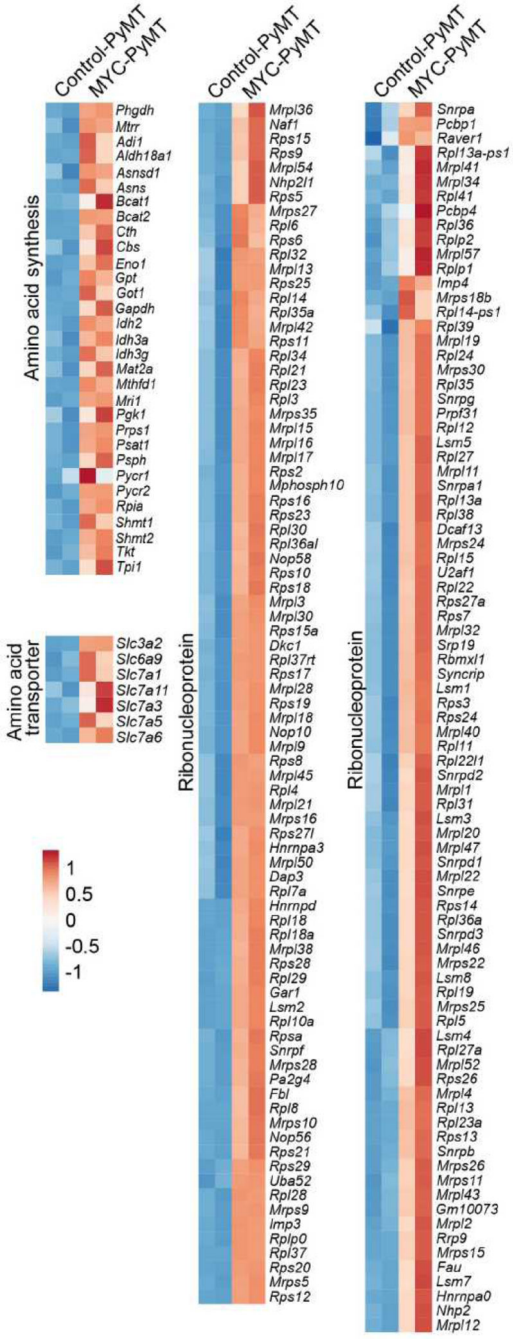

Extended data fig. 2. MYC induces expression of amino acid metabolism genes in PyMT tumors.

A heatmap showing significantly differentially expressed genes (adjusted $P < 0.05$) from RNA-sequencing experiments between *S100a8-cre-Rosa26*$^{LSL\text{-}MYC/+}$PyMT (MYC-PyMT) and control-PyMT tumors, categorized in groups that encode for proteins involved in amino acid synthesis, amino acid transporters, and ribonucleoproteins.

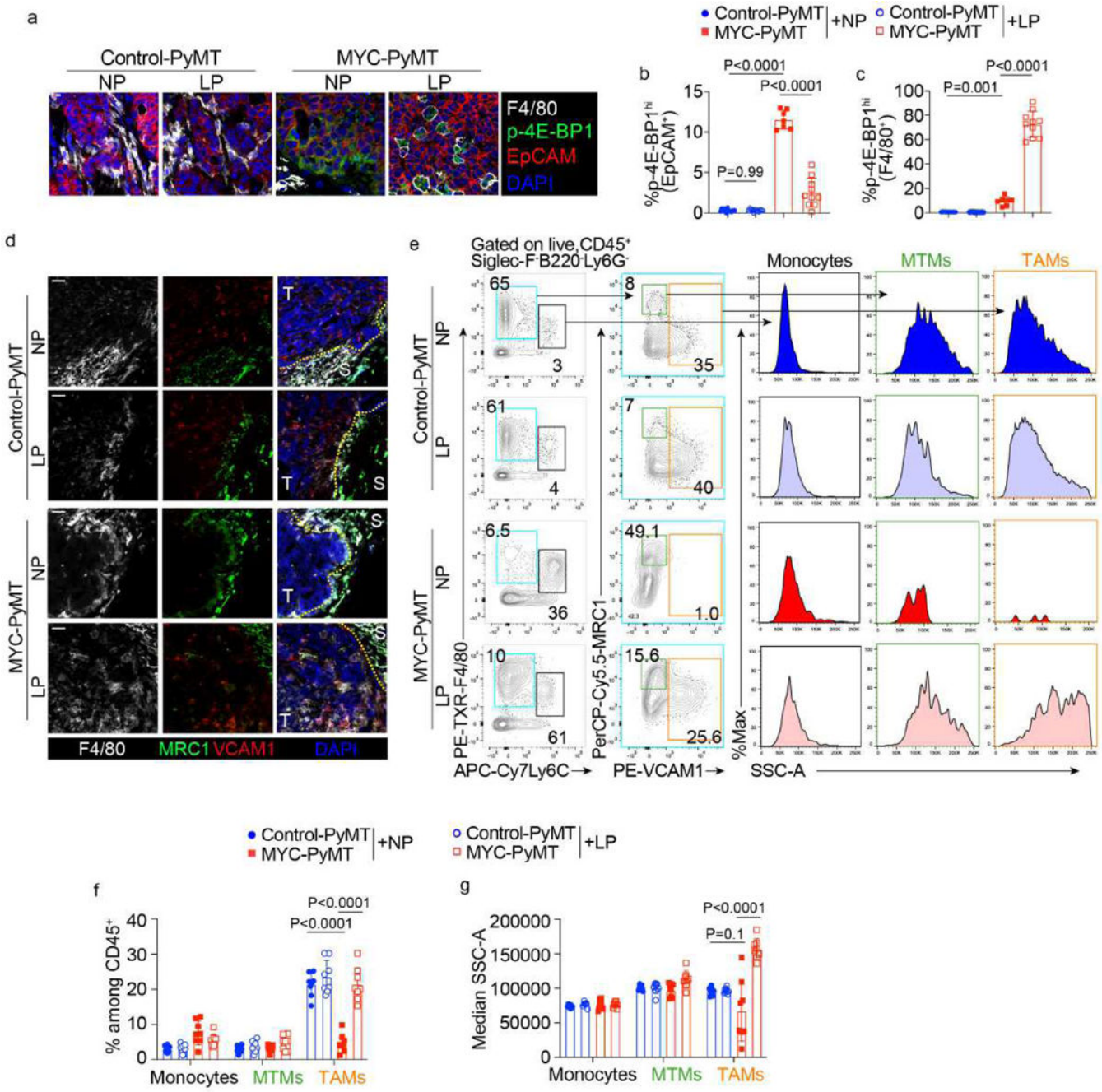

Extended data fig. 3. A low protein diet triggers TAM reprogramming in MYC-PyMT mice.

a, Immunofluorescence images showing expression of F4/80, phosphorylated 4E-BP1 (p-4E-BP1), and EpCAM in 6 mm x 6 mm tumor tissue samples from mice of the indicated genotypes and dietary treatment conditions. Scale bar: 5 μm. **b-c**, Quantification of percentage of cells with high p-4E-BP1 expression among EpCAM-expressing cancer cells and F4/80-expressing macrophages (TAMs) in the tumor parenchyma. n = 12 mice for control-PyMT + NP or LP, n = 7 mice for MYC-PyMT + NP, and n = 10 mice for MYC-PyMT + LP. **d**, Immunofluorescence images showing expression of F4/80, MRC1, and VCAM1 in 6 mm x 6 mm tumor tissue samples from mice of the indicated

genotypes and dietary treatment conditions. MRC1 is highly expressed in mammary tissue macrophages (MTMs) in the tumor interstitial region, while VCAM1 is highly expressed in tumor-associated macrophages (TAMs) residing in the tumor parenchyma. Scale bar: 50 μm. T: tumor parenchyma, S: interstitial region or stroma of the tumor tissue. Parenchyma-interstitial region borders marked by yellow dashed lines. **e-g**, Contour plots and histograms showing the gating strategy and side scatter SSC-A of monocytes, MTMs, and TAMs isolated from mice of the indicated genotypes and dietary treatment conditions. Siglec-F, B220, and Ly6G markers were used to exclude eosinophils, B cells, and neutrophils, respectively. (**e**). The percentage of monocytes, MTMs, and TAMs among $CD45^+$ cells (**f**) and their median SSC-A (**g**) are quantified (n = 8 for each group). NP: control diet with 15% protein in weight (5CC7, TestDiet), LP: low protein diet with 2% protein in weight (5BT9, TestDiet). All statistical data are shown as mean ± S.D. One-way ANOVA with the Tukey multiple comparison test correction in (**b, c, f, g**).

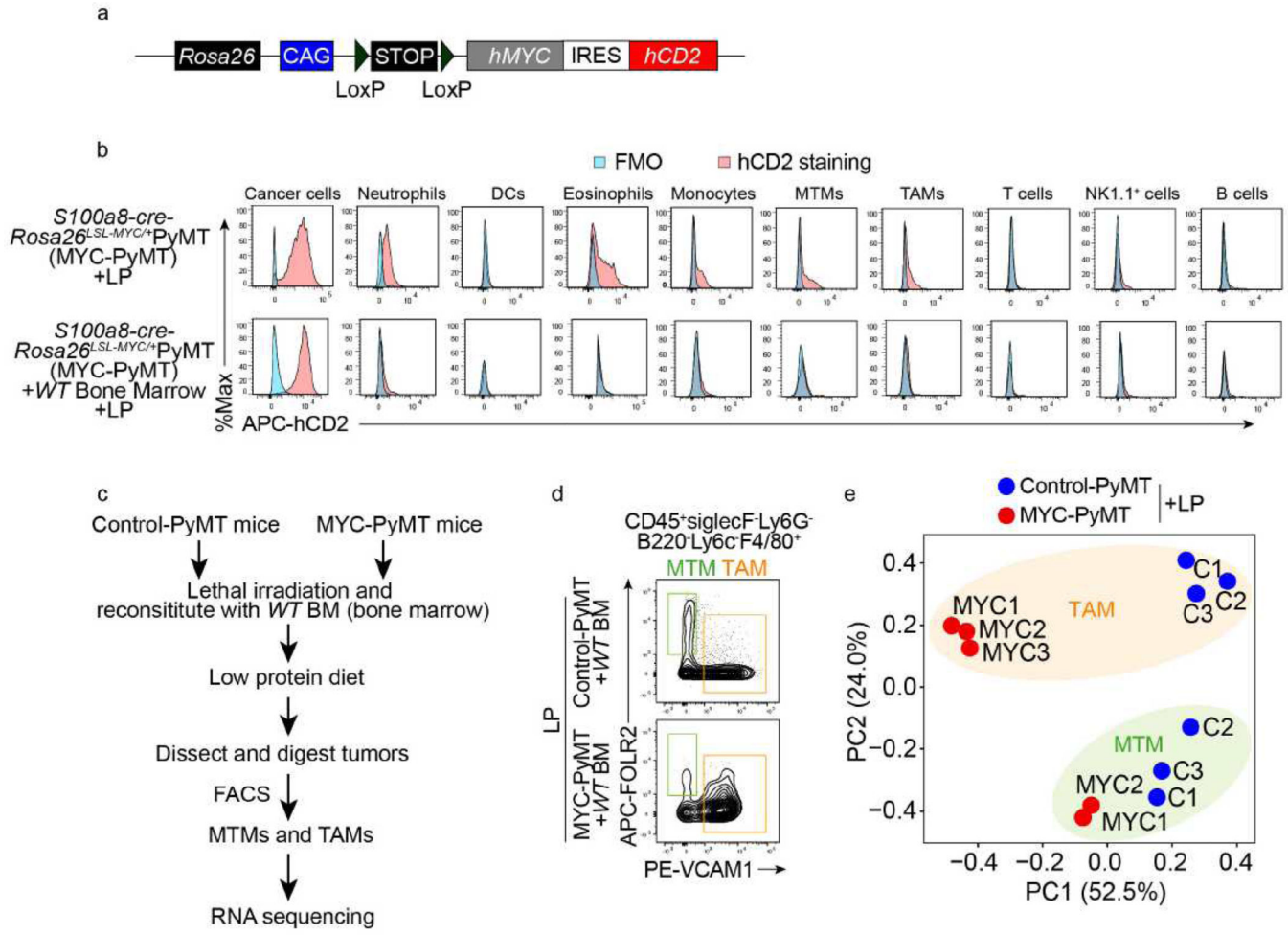

Extended data fig. 4. Transcriptome profiling of TAMs and MTMs.

a, A schematic diagram showing the *Rosa26*$^{LSL\text{-}MYC}$ allele that encodes human MYC (hMYC) and the internal ribosome entry site (IRES)-driven truncated human CD2 (hCD2) protein as a cell surface reporter. **b**, Reporter assay showing the specificity of *S100a8-cre-*

mediated recombination of the *Rosa26*$^{LSL\text{-}MYC}$ allele and high reconstitution efficiency of wild-type (*WT*) bone marrow cells. **c**, Experimental design of bulk RNA-sequencing experiments for tumor-associated macrophages (TAMs) and mammary tissue macrophages (MTMs) isolated from control-PyMT and MYC-PyMT mice reconstituted with *WT* bone marrow cells and treated with a low protein (LP) diet (2% protein in weight, 5BT9, TestDiet). **d**, Flow cytometry gating strategy for TAMs and MTMs. Siglec-F, B220, Ly6G, and Ly6C were used to exclude eosinophils, B cells, neutrophils, and monocytes, respectively. **e**. PCA analysis of TAMs and MTMs isolated from control-PyMT and MYC-PyMT mice reconstituted with *WT* bone marrow cells and treated with a LP diet, based on the log2 fold change of gene expression compared to the mean. MTMs from MYC3 group are not included due to insufficient cell number.

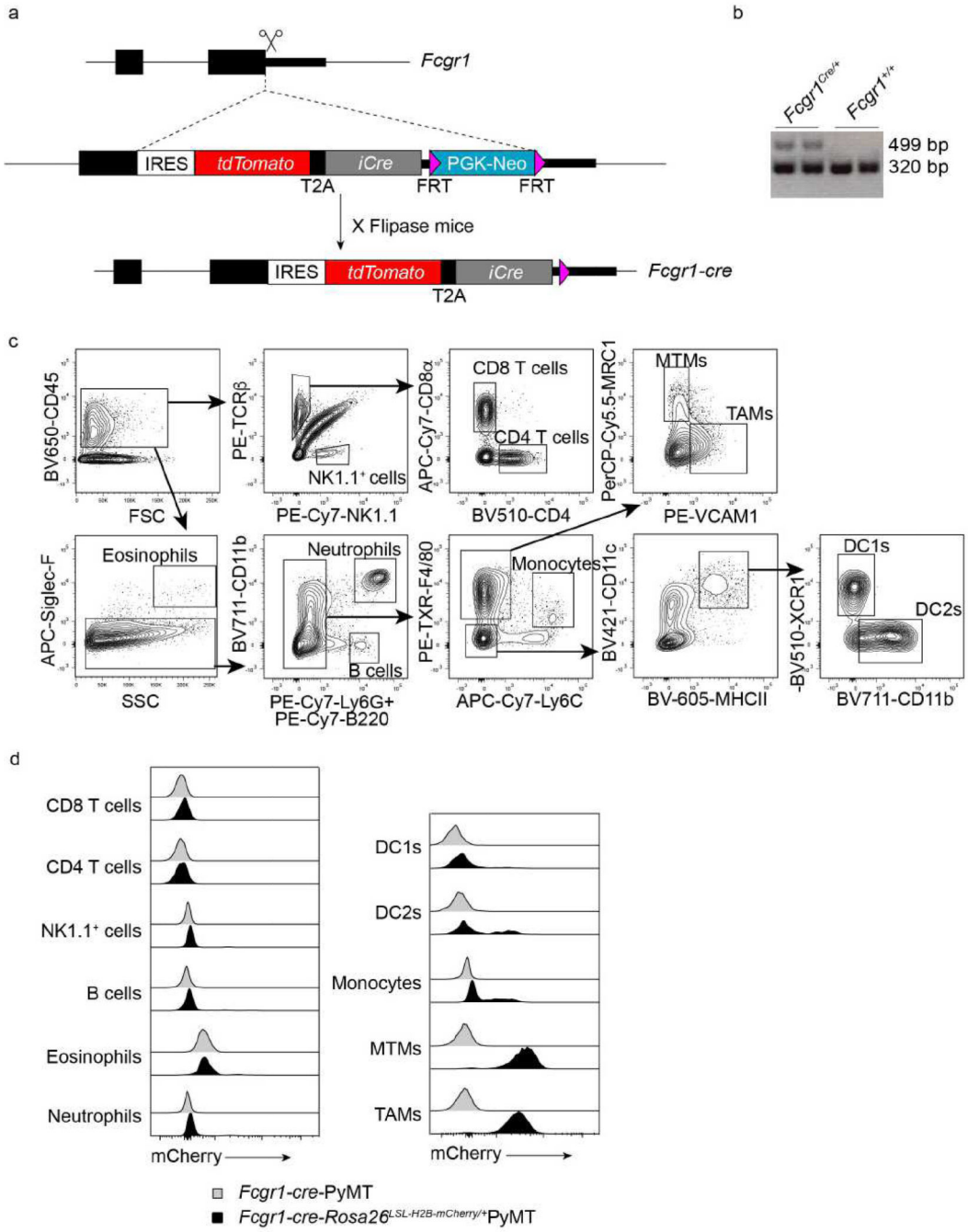

Extended data fig. 5. Generation and validation of *Fcgr1-cre* mice.

a, A schematic diagram showing the design of *Fcgr1-cre* knock-in mice with an IRES-tdTomato-T2A-iCre expression cassette targeted to the *Fcgr1* gene locus. **b**, Validation of the *Fcgr1-cre* knock-in allele by PCR showing germ line transmission of the targeted allele. PCR results were consistently observed across all generations of mice. **c**, **d**, Reporter assay showing the specificity of *Fcgr1-cre*-mediated recombination of the *Rosa26*$^{LSL\text{-}H2B\text{-}mCherry}$ allele. Gating strategy of tumor-infiltrating immune cell populations in (**c**). Top and bottom rows indicate two separate experiments. Histogram overlays in (**d**) showing H2B-

mCherry expression in various tumor-infiltrating immune cell populations isolated from the indicated genotypes. Chromatin-associated H2B-mCherry, but not tdTomato expressed in the cytosol, was retained after fixation and permeabilization in flow cytometric analysis. MTM: mammary tissue macrophage; TAM: tumor-associated macrophage; DC1: type 1 dendritic cell; DC2: type 2 dendritic cell.

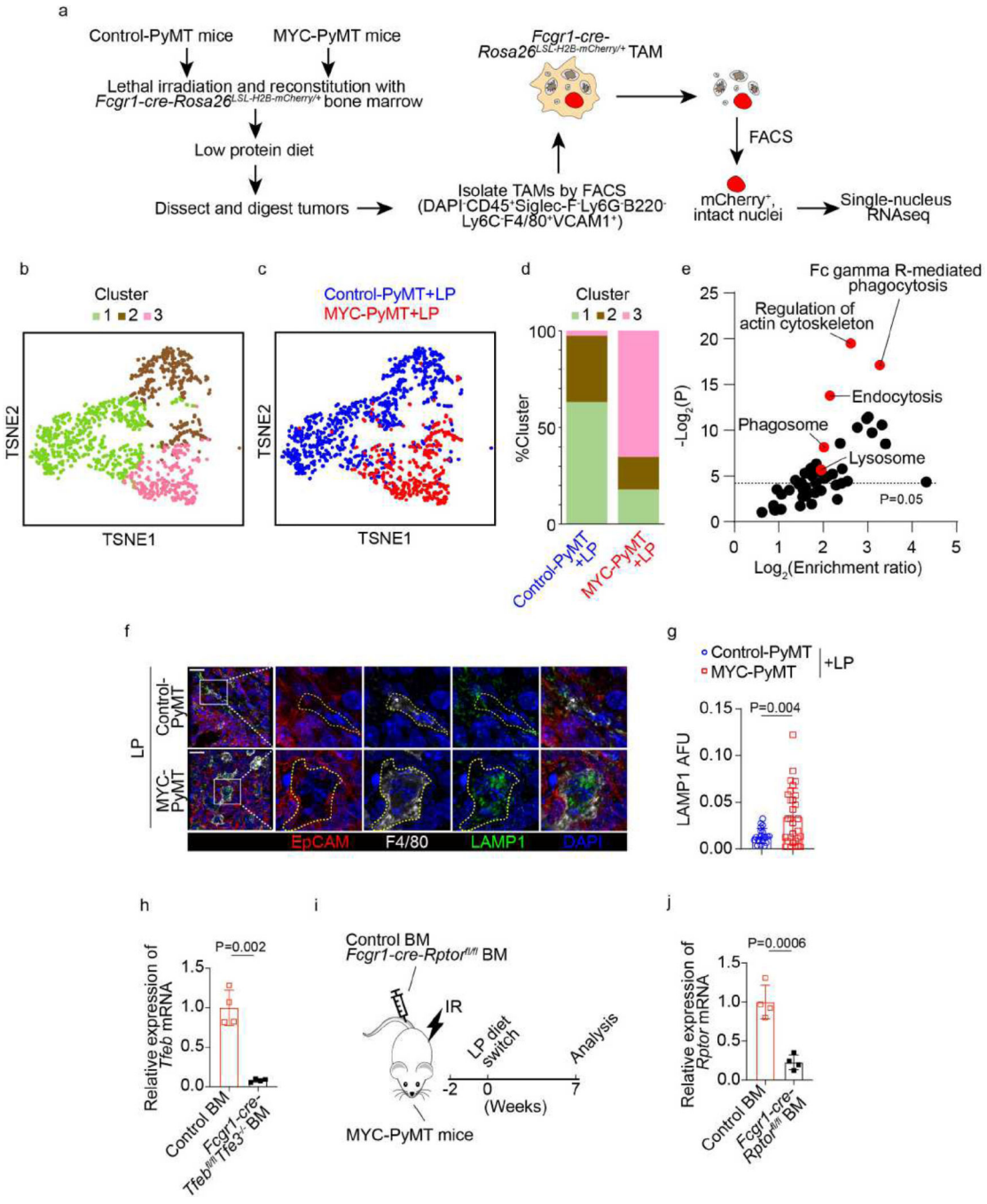

Extended data fig. 6. TAMs are dietarily reprogramed in MYC-PyMT mice.

a, A schematic diagram showing the design of single-nucleus RNA-sequencing experiments in Control-PyMT and MYC-PyMT mice. Siglec-F, B220, Ly6G, and Ly6C were used to exclude eosinophils, B cells, neutrophils, and monocytes, respectively. VCAM1 is a marker for the tumor parenchyma-localized TAMs. **b-d**, TSNE plots showing unsupervised clustering of TAM nuclei isolated from the low protein (LP) diet (2% protein in weight, 5BT9, TestDiet)-conditioned control-PyMT and MYC-PyMT tumors, and color-coded as sub-clusters in (**b**) and genotypes in (**c**). Percentage of each sub-cluster of TAM nuclei from control-PyMT and MYC-PyMT tumors (**d**). **e**, A scatter plot showing enriched gene sets from differentially expressed genes (adjusted $P < 0.05$) in cluster 3 versus other clusters. **f**, Immunofluorescence images showing expression of F4/80, EpCAM, and LAMP in 6 mm x 6 mm tumor tissue samples from the LP diet-treated control-PyMT and MYC-PyMT mice. Scale bar: 20 μm. Representative TAMs marked by yellow dashed lines. **g**, Quantification of AFU (arbitrary fluorescence unit) of LAMP1 expressing in F4/80-expressing TAMs from the LP diet-treated control-PyMT and MYC-PyMT mice (n = 3 mice for control-PyMT + LP, n = 4 mice for MYC-PyMT + LP). Data points are average AFU from each captured images. **h, j**, RT-qPCR analysis of *Tfeb* and *Rptor* mRNA expression in TAMs of the indicated genotypes (n = 4 mice for each group). **i**, A schematic diagram showing the generation of bone marrow (BM) chimera mice. BM cells from control, *Fcgr1-cre-Rptor*$^{fl/fl}$ mice were transferred into lethally irradiated MYC-PyMT recipients with a tumor burden around 250–350 mm^3 followed by switching to the LP diet two weeks after. All statistical data are shown as mean ± S.D. Over-representation analysis based on hypergeometric test with the Benjamini-Hochberg multiple comparison test correction in (**e**), two-sided Student t-test in (**g, h, j**).

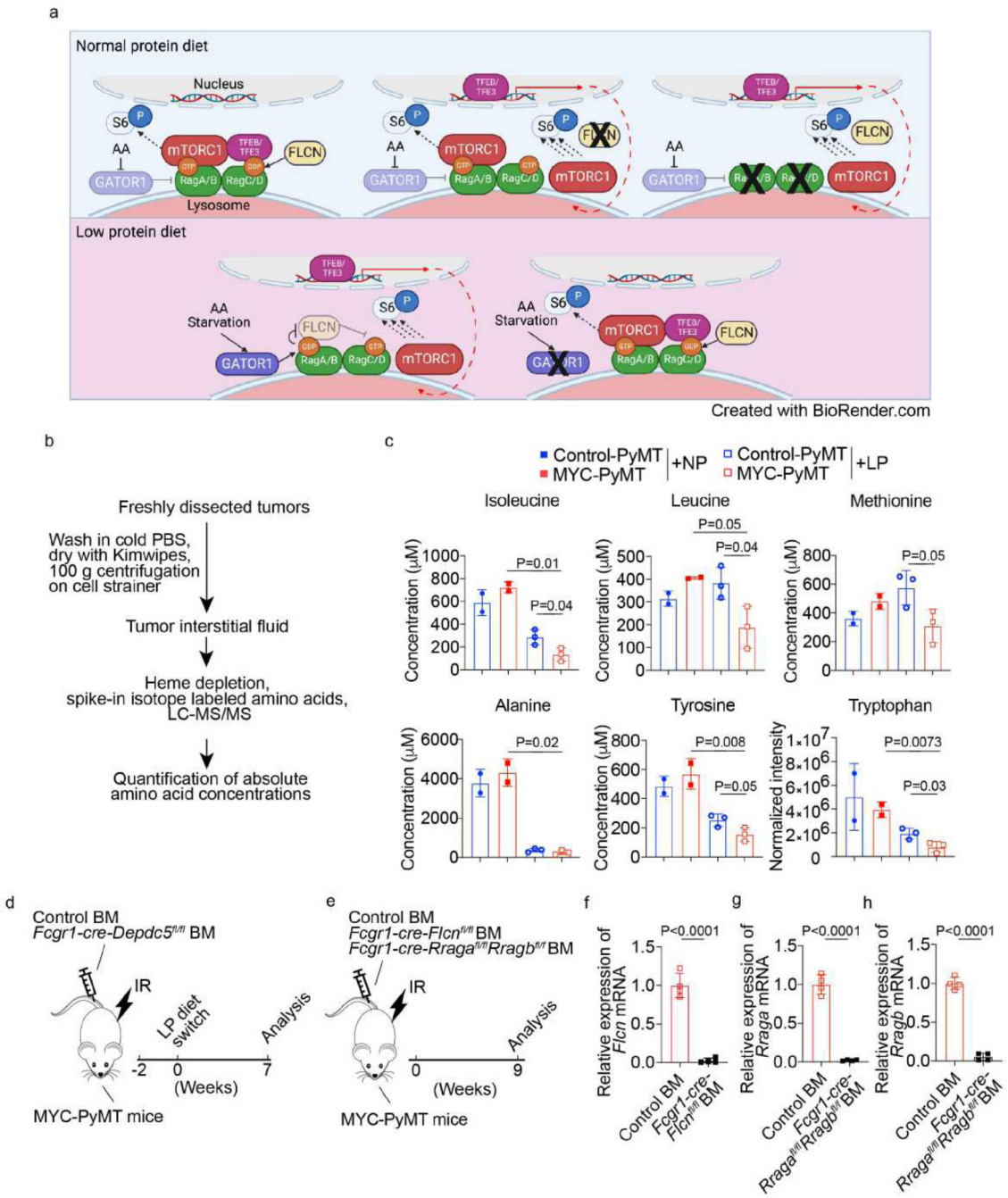

Extended data fig. 7. Two modes of mTORC1 signaling promoted or suppressed by Rag GTPases.

a. A schematic diagram showing two modes of mTORC1 signaling in TAMs promoted or suppressed by Rag GTPases. Under a normal protein (NP) diet (15% protein in weight, 5CC7, TestDiet) condition, abundant cytosolic amino acids (AAs) suppress the GATOR1 complex, but activate the FLCN complex, and induce Rag GTPases in a RagA/B^{GTP}-RagC/D^{GDP} state that recruits mTORC1 and TFEB/TFE3 to the Rag GTPase complex, supporting or inhibiting their activation, respectively. Under a low protein (LP) diet (2% protein in

weight, 5BT9, TestDiet) condition, AA starvation activates GATOR1, but inactivates FLCN, and induces Rag GTPases in a RagA/B^{GDP}-RagC/D^{GTP} state that dissociates mTORC1 and TFEB/TFE3 from the Rag GTPase complex, leading to TFEB/TFE3 nuclear translocation and mTORC1 activation through Rag GTPase-independent mechanisms. Depletion of GATOR1 maintains a RagC/D^{GDP} state under the LP diet condition, while depletion of FLCN maintains a RagC/D^{GTP} state under the NP diet condition, causing inaction or activation of the TFEB/TFE3-mTORC1 signaling pathway, respectively. Depletion of Rag GTPases also activates TFEB/TFE3-mTORC1 signaling under the NP diet condition. **b**, **c**, Mass spectrometry quantification of individual AAs in tumor interstitial fluid extracted from control-PyMT and MYC-PyMT tumors under NP or LP diet conditions. AAs shown changes in the LP diet-treated MYC-PyMT tumors were plotted. Due to the absence of spike-in isotope labeled tryptophan, normalized intensity was shown. n = 2 mice each condition for NP treated control-PyMT and MYC-PyMT, and n = 3 mice each condition for LP treated control-PyMT and MYC-PyMT. **d**, A schematic diagrams showing the generation of bone marrow (BM) chimera mice. BM cells from control *and Fcgr1-cre-Depdc5*$^{fl/fl}$ mice were transferred into lethally irradiated MYC-PyMT recipients with a tumor burden around 250–350 mm^3 followed by switching to the LP diet two weeks after. **e**, BM cells from control, *Fcgr1-cre-Flcn*$^{fl/fl}$, and *Fcgr1-cre-Rraga*$^{fl/fl}$*Rragb*$^{fl/fl}$ mice were transferred into lethally irradiated MYC-PyMT recipients with a tumor burden around 250–350 mm^3 and kept under the NP diet condition. **f-h**, RT-qPCR analysis of *Flcn*, *Rraga*, and *Rragb* mRNA expression in TAMs of the indicated genotypes (n = 4 mice for each group). All statistical data are shown as mean ± S.D. Two-sided Student t-test in (**c**, **f-h**).

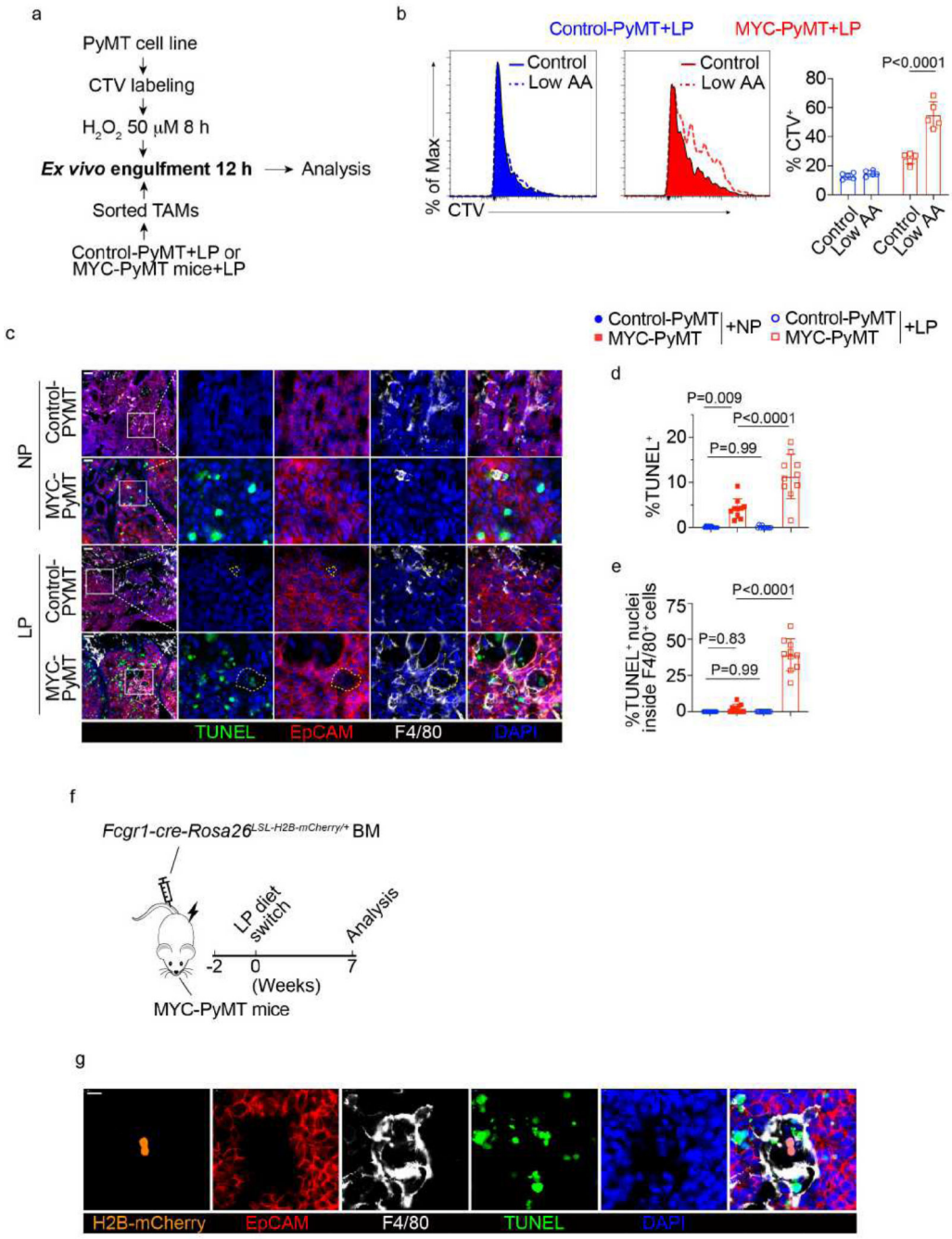

Extended data fig. 8. Dietarily reprogramed TAMs engulf apoptotic cells in MYC-PyMT tumors.

a, b, Experimental design, flow cytometric analysis and quantification of TAM engulfment of apoptotic cells in a complete or low amino acid (AA) RPMI medium (1: 4 mixture of complete RPMI and AA-free RPMI). Apoptotic PyMT cancer cells were labeled by CellTrace Violet (CTV) and induced by H_2O_2 treatment. TAMs were isolated from tumors of control-PyMT and MYC-PyMT mice (n=5 for each group) treated with a low protein (LP) diet (2% protein in weight, 5BT9, TestDiet). **c**, Immunofluorescence images showing expression or localization of F4/80, EpCAM, and TUNEL in 6 mm x 6 mm tumors from

control-PyMT and MYC-PyMT mice under LP or normal protein (NP) diet (15% protein in weight, 5CC7, TestDiet) conditions. Scale bar: 50 μm. Representative macrophages marked by yellow dashed lines. **d**, Quantification of percentage of TUNEL-positive cells among all cells. **e**, Quantification of percentage of TUNEL-positive nuclei inside F4/80-expressing macrophages. Data points are average percentage from random captured images. n = 3 mice for each group in (**d**, **e**). **f**, A schematic diagram showing the generation of bone marrow (BM) chimera mice. BM cells from *Fcgr1-cre-Rosa26*$^{LSL\text{-}H2B\text{-}mCherry/+}$ mice were transferred into lethally irradiated MYC-PyMT recipients with a tumor burden around 250–350 mm^3 followed by switching to the LP diet two weeks after. **g**, Immunofluorescence images showing expression or localization of F4/80, EpCAM, H2B-mCherry, and TUNEL in 6 mm x 6 mm tumor tissue samples from BM chimera mice described in (**f**). Scale bar: 10 μm. All statistical data are shown as mean ± S.D. One-way ANOVA with the Tukey multiple comparison test correction in (**b, d**, **e**).

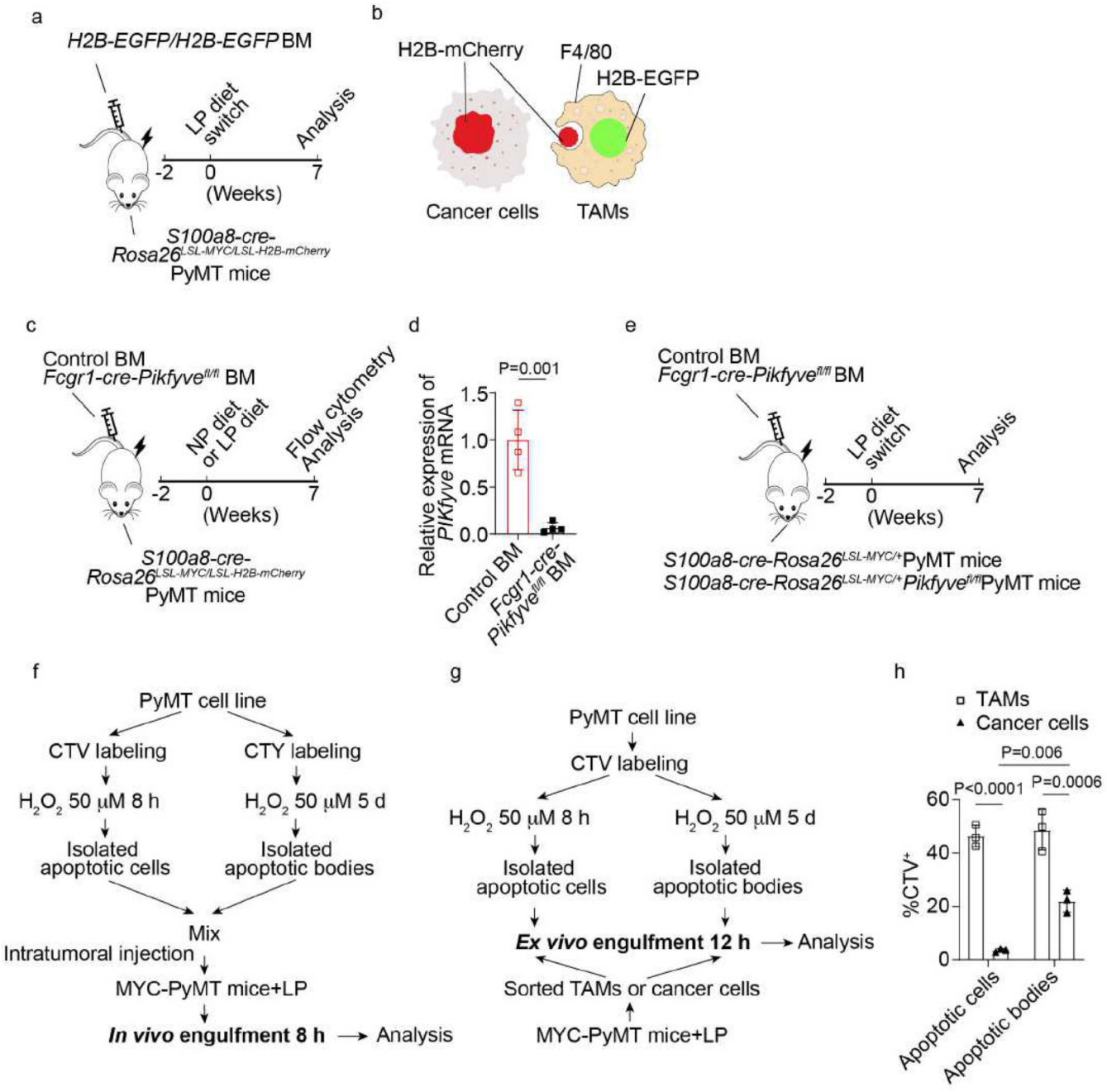

Extended data fig. 9. Apoptotic cancer cells are effectively phagocytosed by reprogramed TAMs.

a, **b**, Schematic diagrams showing bone marrow (BM) chimera mice to define TAM engulfment of dying cancer cells. BM cells from homozygous *H2B-EGFP/H2B-EGFP* mice were transferred into lethally irradiated *S100a8-cre-Rosa26*$^{LSL\text{-}MYC/LSL\text{-}H2B\text{-}mCherry}$PyMT recipients with a tumor burden around 250–350 mm^3 followed by switching to a low protein (LP) diet (2% protein in weight, 5BT9, TestDiet) two weeks after. **c**, A schematic diagram showing dietary treatment of BM chimera mice. BM cells of control or *Fcgr1-cre-Pikfyve*$^{fl/fl}$ mice were transferred into lethally irradiated *S100a8-cre-Rosa26*$^{LSL\text{-}MYC/LSL\text{-}H2B\text{-}mcherry}$PyMT recipients with a tumor burden around 250–350 mm^3,

which were either kept under a normal protein (NP) diet (15% protein in weight, 5CC7, TestDiet) condition or switched to a LP diet two weeks after. **d**, RT-qPCR analysis of *PIKfyve* mRNA expression in TAMs of the indicated genotypes (n = 4 mice for each group). **e**, A schematic diagram showing dietary treatment of BM chimera mice. BM cells from control or *Fcgr1-cre-Pikfyve*$^{fl/fl}$ mice were transferred into lethally irradiated *S100a8-cre-Rosa26*$^{LSL\text{-}MYC/+}$PyMT or *S100a8-cre-Rosa26*$^{LSL\text{-}MYC/+}$*Pikfyve*$^{fl/fl}$PyMT recipients with a tumor burden around 250–350 mm^3 followed by switching to a LP diet two weeks after. **f**, Experimental design of an *in vivo* engulfment assay with intratumoral injection of CellTrace Violet (CTV) and CellTrace Yellow (CTY)-labeled apoptotic cells and apoptotic bodies. **g, h**, Experimental design and flow cytometry analysis of an *ex vivo* engulfment assay with TAMs and cancer cells fed with apoptotic cells and apoptotic bodies in a low amino acid RPMI medium (1: 4 mixtures of RPMI and amino acid-free RPMI). n = 3 independent experiments and cells from independent mice each group. All statistical data are shown as mean ± S.D. Two-sided Student t-test in (**d**), one-way ANOVA with the Tukey multiple comparison test correction in (**h**).

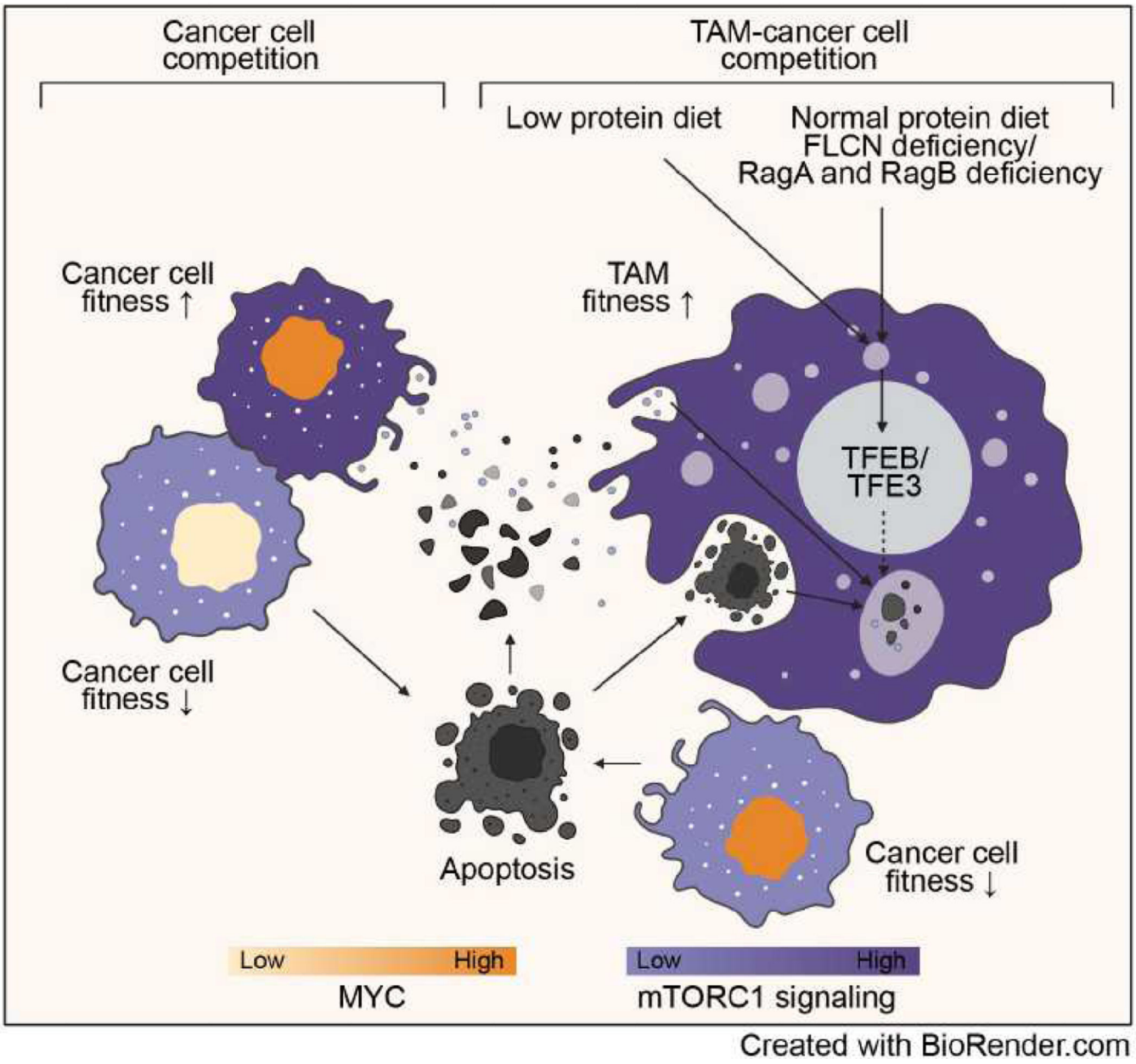

Extended data fig. 10. Reprogram TAMs to outmatch cancer cell competition.

In *S100a8-cre-Rosa26*$^{LSL\text{-}MYC/+}$PyMT mice, MYC^{hi} cancer cells are fitter than MYC^{lo} cancer cells and outcompete them in a process dependent on higher mTORC1 signaling. Cell debris from apoptotic cancer cells are acquired by MYC^{hi} cancer cells as a nutrient source to promote mTORC1 activation and the 'winner' status. Feeding mice with a low protein diet or depletion of FLCN or Rag GTPases activates TFEB/TFE3 and mTORC1 signaling in tumor-associated macrophages (TAMs) and enhances TAM fitness supported by engulfment of apoptotic cancer cells and apoptotic cell debris. Such a contest in engulfment-dependent nutrient acquisition dictates cell competition between TAMs and MYC^{hi} cancer cells, which defines an innate immune tumor suppression pathway that may be targeted for cancer immunotherapy.

Supplementary Material

Refer to Web version on PubMed Central for supplementary material.

Acknowledgement

We thank members of the M.O.L. laboratory for helpful discussions. This work was supported by Howard Hughes Medical Institute (Faculty Scholar Award to M.O.L.), MSKCC Geoffrey Beene Cancer Research Center (M.O.L.), MSKCC Alan and Sandra Gerry Metastasis and Tumor Ecosystems Center (M.O.L.), the Mazumdar-Shaw Translational Research Initiative in Kidney Cancer (M.O.L.), Cancer Research Institute (Irvington Fellow awards to X.Z., S.L., C.C., L.J.), MSKCC Cancer Center Support Grant (P30 CA08748), and Federal funds from the National Cancer Institute and National Institutes of Health, under Contract No. HHSN261201500003I (L.S.S.). We also thank Integrated Genomics Operation Core at MSKCC, Cycle for Survival and the Marie-Josée and Henry R. Kravis Center for Molecular Oncology. We acknowledge NYU Langone Health's Metabolomics Laboratory, partially supported by the Cancer Center Support Grant P30CA016087 at the Laura and Isaac Perlmutter Cancer Center, for acquiring and analyzing the amino acid profiling data. We thank Mariano Aufiero and Tobias Hohl at MSKCC for transferring key mouse lines. All illustrations were created with BioRender.com.

Data Availability

All the data of this study are available in the article, extended data and supplementary data. All the data from next generation sequencing experiments can be accessed from GSE230244, GSE230245, GSE230247.

References

1. Baker NE Emerging mechanisms of cell competition. Nat Rev Genet 21, 683–697 (2020). [PubMed: 32778819]
2. Neerven SM van & Vermeulen L. Cell competition in development, homeostasis and cancer. Nat Rev Mol Cell Bio 1–16 (2022) doi:10.1038/s41580-022-00538-y.
3. Johnston LA Socializing with MYC: Cell Competition in Development and as a Model for Premalignant Cancer. Csh Perspect Med 4, a014274 (2014).
4. Paglia S, Sollazzo M, Giacomo SD, Strocchi S. & Grifoni D. Exploring MYC relevance to cancer biology from the perspective of cell competition. Semin Cancer Biol 63, 49–59 (2020). [PubMed: 31102666]
5. Vishwakarma M. & Piddini E. Outcompeting cancer. Nat Rev Cancer 20, 187–198 (2020). [PubMed: 31932757]
6. Marongiu F, Cheri S. & Laconi E. Cell competition, cooperation, and cancer. Neoplasia 23, 1029–1036 (2021). [PubMed: 34500336]
7. Lau AN & Heiden MGV Metabolism in the Tumor Microenvironment. Annu Rev Cancer Biology 4, 1–24 (2019).
8. Faubert B, Solmonson A. & DeBerardinis RJ Metabolic reprogramming and cancer progression. Science 368, (2020).
9. Bar-Peled L. et al. A Tumor Suppressor Complex with GAP Activity for the Rag GTPases That Signal Amino Acid Sufficiency to mTORC1. Science 340, 1100–1106 (2013). [PubMed: 23723238]
10. Tsun Z-Y et al. The Folliculin Tumor Suppressor Is a GAP for the RagC/D GTPases That Signal Amino Acid Levels to mTORC1. Mol Cell 52, 495–505 (2013). [PubMed: 24095279]
11. Lawrence RE et al. Structural mechanism of a Rag GTPase activation checkpoint by the lysosomal folliculin complex. Science 366, 971–977 (2019). [PubMed: 31672913]
12. Martina JA & Puertollano R. Rag GTPases mediate amino acid–dependent recruitment of TFEB and MITF to lysosomes. J Cell Biol 200, 475–491 (2013). [PubMed: 23401004]
13. Napolitano G. et al. A substrate-specific mTORC1 pathway underlies Birt–Hogg–Dubé syndrome. Nature 585, 597–602 (2020). [PubMed: 32612235]

14. Li K. et al. Folliculin promotes substrate-selective mTORC1 activity by activating RagC to recruit TFE3. Plos Biol 20, e3001594 (2022).
15. de la Cova C, Abril M, Bellosta P, Gallant P. & Johnston LA Drosophila Myc Regulates Organ Size by Inducing Cell Competition. Cell 117, 107–116 (2004). [PubMed: 15066286]
16. Moreno E. & Basler K. dMyc Transforms Cells into Super-Competitors. Cell 117, 117–129 (2004). [PubMed: 15066287]
17. Clavería C, Giovinazzo G, Sierra R. & Torres M. Myc-driven endogenous cell competition in the early mammalian embryo. Nature 500, 39–44 (2013). [PubMed: 23842495]
18. Sancho M. et al. Competitive Interactions Eliminate Unfit Embryonic Stem Cells at the Onset of Differentiation. Dev Cell 26, 19–30 (2013). [PubMed: 23867226]
19. Dang CV MYC on the Path to Cancer. Cell 149, 22–35 (2012). [PubMed: 22464321]
20. Dhanasekaran R. et al. The MYC oncogene — the grand orchestrator of cancer growth and immune evasion. Nat Rev Clin Oncol 19, 23–36 (2022). [PubMed: 34508258]
21. Schaub FX et al. Pan-cancer Alterations of the MYC Oncogene and Its Proximal Network across the Cancer Genome Atlas. Cell Syst 6, 282–300.e2 (2018). [PubMed: 29596783]
22. Giacomo SD et al. Human Cancer Cells Signal Their Competitive Fitness Through MYC Activity. Sci Rep-uk 7, 12568 (2017).
23. McMahon SB MYC and the Control of Apoptosis. Csh Perspect Med 4, a014407 (2014).
24. Giacomo SD, Sollazzo M, Paglia S. & Grifoni D. MYC, Cell Competition, and Cell Death in Cancer: The Inseparable Triad. Genes-basel 8, 120 (2017). [PubMed: 28420161]
25. Ichaso N. & Dilworth SM Cell transformation by the middle T-antigen of polyoma virus. Oncogene 20, 7908–7916 (2001). [PubMed: 11753673]
26. Kansler ER et al. Cytotoxic innate lymphoid cells sense cancer cell-expressed interleukin-15 to suppress human and murine malignancies. Nat Immunol 23, 904–915 (2022). [PubMed: 35618834]
27. Bowling S. et al. P53 and mTOR signalling determine fitness selection through cell competition during early mouse embryonic development. Nat Commun 9, 1763 (2018). [PubMed: 29720666]
28. Bar-Peled L. & Sabatini DM Regulation of mTORC1 by amino acids. Trends Cell Biol 24, 400–406 (2014). [PubMed: 24698685]
29. Dibble CC & Cantley LC Regulation of mTORC1 by PI3K signaling. Trends Cell Biol 25, 545–555 (2015). [PubMed: 26159692]
30. Zhang X, Ji L. & Li MO Control of tumor-associated macrophage responses by nutrient acquisition and metabolism. Immunity 56, 14–31 (2023). [PubMed: 36630912]
31. Franklin RA et al. The cellular and molecular origin of tumor-associated macrophages. Science 344, 921–925 (2014). [PubMed: 24812208]
32. Sardiello M. et al. A Gene Network Regulating Lysosomal Biogenesis and Function. Science 325, 473–477 (2009). [PubMed: 19556463]
33. Settembre C. et al. TFEB Links Autophagy to Lysosomal Biogenesis. Science 332, 1429–1433 (2011). [PubMed: 21617040]
34. Martina JA et al. The Nutrient-Responsive Transcription Factor TFE3 Promotes Autophagy, Lysosomal Biogenesis, and Clearance of Cellular Debris. Sci Signal 7, ra9 (2014).
35. Puertollano R, Ferguson SM, Brugarolas J. & Ballabio A. The complex relationship between TFEB transcription factor phosphorylation and subcellular localization. Embo J 37, (2018).
36. Peng M, Yin N. & Li MO Sestrins Function as Guanine Nucleotide Dissociation Inhibitors for Rag GTPases to Control mTORC1 Signaling. Cell 159, 122–133 (2014). [PubMed: 25259925]
37. Wolfson RL et al. Sestrin2 is a leucine sensor for the mTORC1 pathway. Science 351, 43–48 (2016). [PubMed: 26449471]
38. Peng M, Yin N. & Li MO SZT2 dictates GATOR control of mTORC1 signalling. Nature 543, 433–437 (2017). [PubMed: 28199315]
39. Shi H. et al. Amino Acids License Kinase mTORC1 Activity and Treg Cell Function via Small G Proteins Rag and Rheb. Immunity 51, 1012–1027.e7 (2019). [PubMed: 31668641]
40. Do MH et al. Nutrient mTORC1 signaling underpins regulatory T cell control of immune tolerance. J Exp Med 217, (2020).

41. Hesketh GG et al. The GATOR–Rag GTPase pathway inhibits mTORC1 activation by lysosome-derived amino acids. Science 370, 351–356 (2020). [PubMed: 33060361]
42. Kim GHE, Dayam RM, Prashar A, Terebiznik M. & Botelho RJ PIKfyve Inhibition Interferes with Phagosome and Endosome Maturation in Macrophages. Traffic 15, 1143–1163 (2014). [PubMed: 25041080]
43. Krishna S. et al. PIKfyve Regulates Vacuole Maturation and Nutrient Recovery following Engulfment. Dev Cell 38, 536–547 (2016). [PubMed: 27623384]
44. Min SH et al. PIKfyve Deficiency in Myeloid Cells Impairs Lysosomal Homeostasis in Macrophages and Promotes Systemic Inflammation in Mice. Mol Cell Biol 39, (2019).
45. Kawasaki T, Ito K, Miyata H, Akira S. & Kawai T. Deletion of PIKfyve alters alveolar macrophage populations and exacerbates allergic inflammation in mice. Embo J 36, 1707–1718 (2017). [PubMed: 28533230]
46. Eichenlaub T, Cohen SM & Herranz H. Cell Competition Drives the Formation of Metastatic Tumors in a Drosophila Model of Epithelial Tumor Formation. Curr Biol 26, 419–427 (2016). [PubMed: 26853367]
47. Commisso C. et al. Macropinocytosis of protein is an amino acid supply route in Ras-transformed cells. Nature 497, 633–637 (2013). [PubMed: 23665962]
48. Jayashankar V. & Edinger AL Macropinocytosis confers resistance to therapies targeting cancer anabolism. Nat Commun 11, 1121 (2020). [PubMed: 32111826]
49. Palm W. et al. The Utilization of Extracellular Proteins as Nutrients Is Suppressed by mTORC1. Cell 162, 259–270 (2015). [PubMed: 26144316]
50. Nixon BG et al. Tumor-associated macrophages expressing the transcription factor IRF8 promote T cell exhaustion in cancer. Immunity (2022) doi:10.1016/j.immuni.2022.10.002.

Methods References

51. Calado DP et al. MYC is essential for the formation and maintenance of germinal centers. Nat Immunol 13, 1092–1100 (2012). [PubMed: 23001146]
52. Passegué E, Wagner EF & Weissman IL JunB Deficiency Leads to a Myeloproliferative Disorder Arising from Hematopoietic Stem Cells. Cell 119, 431–443 (2004). [PubMed: 15507213]
53. Sengupta S, Peterson TR, Laplante M, Oh S. & Sabatini DM mTORC1 controls fasting-induced ketogenesis and its modulation by ageing. Nature 468, 1100–1104 (2010). [PubMed: 21179166]
54. Ikonomov OC et al. The Phosphoinositide Kinase PIKfyve Is Vital in Early Embryonic Development PREIMPLANTATION LETHALITY OF PIKfyve−/− EMBRYOS BUT NORMALITY OF PIKfyve+/− MICE*. J Biol Chem 286, 13404–13413 (2011). [PubMed: 21349843]
55. Hadjantonakis A-K & Papaioannou VE Dynamic in vivo imaging and cell tracking using a histone fluorescent protein fusion in mice. Bmc Biotechnol 4, 33 (2004). [PubMed: 15619330]
56. Peron SP, Freeman J, Iyer V, Guo C. & Svoboda K. A Cellular Resolution Map of Barrel Cortex Activity during Tactile Behavior. Neuron 86, 783–799 (2015). [PubMed: 25913859]
57. Efeyan A. et al. RagA, but Not RagB, Is Essential for Embryonic Development and Adult Mice. Dev Cell 29, 321–329 (2014). [PubMed: 24768164]
58. Steingrímsson E. et al. Mitf and Tfe3, two members of the Mitf-Tfe family of bHLH-Zip transcription factors, have important but functionally redundant roles in osteoclast development. Proc National Acad Sci 99, 4477–4482 (2002).
59. Baba M. et al. Kidney-Targeted Birt-Hogg-Dubé Gene Inactivation in a Mouse Model: Erk1/2 and Akt-mTOR Activation, Cell Hyperproliferation, and Polycystic Kidneys. Jnci J National Cancer Inst 100, 140–154 (2008).
60. Settembre C. et al. A lysosome-to-nucleus signalling mechanism senses and regulates the lysosome via mTOR and TFEB. Embo J 31, 1095–1108 (2012). [PubMed: 22343943]
61. Farley FW, Soriano P, Steffen LS & Dymecki SM Widespread recombinase expression using FLPeR (Flipper) mice. Genesis 28, 106–110 (2000). [PubMed: 11105051]

62. Chou C. et al. Programme of self-reactive innate-like T cell-mediated cancer immunity. Nature 605, 139–145 (2022). [PubMed: 35444279]

63. Ramos RN et al. Tissue-resident FOLR2+ macrophages associate with CD8+ T cell infiltration in human breast cancer. Cell (2022) doi:10.1016/j.cell.2022.02.021.

64. Cerami E. et al. The cBio Cancer Genomics Portal: An Open Platform for Exploring Multidimensional Cancer Genomics Data. Cancer Discov 2, 401–404 (2012). [PubMed: 22588877]

65. Gao J. et al. Integrative Analysis of Complex Cancer Genomics and Clinical Profiles Using the cBioPortal. Sci Signal 6, pl1 (2013).

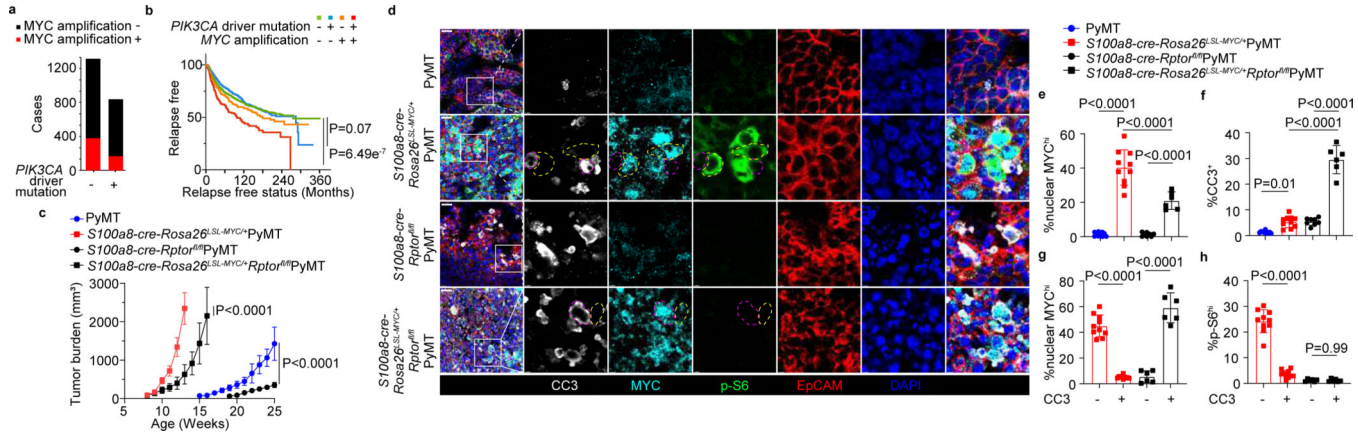

Fig. 1. mTORC1 signaling supports a 'winner' state of MYC^{hi} cancer cells.

a, A bar graph showing the distribution of human breast cancer patient cases with or without *MYC* amplification and/or *PIK3CA* gain-of-function driver mutation from the METABRIC dataset. **b**, A Kaplan Meier relapse free survival graph of human breast cancer patients categorized into groups with none, either or both of *MYC* amplification and *PIK3CA* driver mutation. P-values of log rank test were calculated by comparing all four groups or three groups excluding cooccurrence of *MYC* amplification and *PIK3CA* driver mutation. **c**, Tumor burden in mice of the indicated genotypes including PyMT (n = 5), *S100a8-cre-Rosa26*$^{LSL\text{-}MYC/+}$PyMT (n = 5), *S100a8-cre-Rptor*$^{fl/fl}$PyMT (n = 5), and *S100a8-cre-Rosa26*$^{LSL\text{-}MYC/+}$*Rptor*$^{fl/fl}$PyMT (n = 4). **d**, Immunofluorescence images showing expression of cleaved caspase 3 (CC3), MYC, phosphorylated S6 ribosomal protein at serine 240/244 (p-S6), and EpCAM in 6 mm x 6 mm tumor tissue samples from mice of the indicated genotypes. Scale bar: 20 μm. Representative 'loser' cells marked by magenta dashed lines and 'winner' cells marked by yellow dashed lines. **e**, **f**, Quantification of percentage of cells with high nuclear MYC expression or positive CC3 expression among EpCAM-expressing cancer cells. **g**, **h**, Quantification of percentage of cells with high MYC or p-S6 expression among CC3-positive or −negative EpCAM-expressing cancer cells. In (**e-h**), n = 10 mice for PyMT and *S100a8-cre-Rosa26*$^{LSL\text{-}MYC/+}$PyMT, n = 8 mice for *S100a8-cre-Rptor*$^{fl/fl}$PyMT, and n = 6 mice for *S100a8-cre-Rosa26*$^{LSL\text{-}MYC/+}$*Rptor*$^{fl/fl}$PyMT. All statistical data are shown as mean ± S.D. Two-way ANOVA in (**c**), one-way ANOVA with the Tukey multiple comparison test correction in (**e-h**).

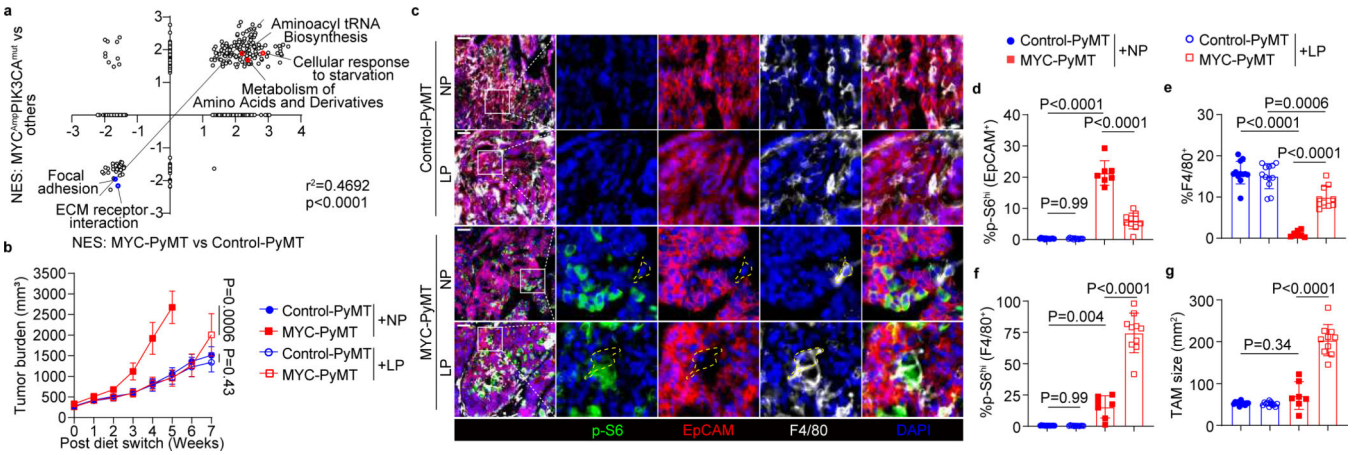

Fig. 2. A low protein diet triggers discordant mTORC1 activation in cancer cells and TAMs.

a, A scatter plot with linear correlation trend line showing enriched gene sets overlapped between human and mouse tumor samples. **b**, Tumor burden in mice of the indicated genotypes under normal protein (NP) or low protein (LP) diet conditions, including control-PyMT + NP (n = 4), control-PyMT + LP (n = 6), MYC-PyMT + NP (n = 5), MYC-PyMT + LP (n = 5). Mice with tumor burden around 250–350 mm^3 from each genotype were treated with the LP diet or kept with the NP diet. **c**, Immunofluorescence images showing expression of phosphorylated S6 ribosomal protein at serine 240/244 (p-S6), EpCAM, and F4/80 in 6 mm x 6 mm tumor tissue samples from mice of the indicated genotypes and dietary treatment conditions. Scale bar: 50 μm. Representative macrophages marked by yellow dashed lines. **d**, Quantification of percentage of cells with high p-S6 expression among EpCAM-expressing cancer cells. **e**, Quantification of percentage of F4/80-expressing macrophages in the tumor parenchyma. **f**, Quantification of percentage of cells with high p-S6 expression among F4/80-expressing macrophages. **g**, Quantification of cell size of F4/80-expressing macrophages. In (**d**-**g**), n = 12 mice for control-PyMT + NP or LP, n = 7 mice for MYC-PyMT + NP, and n = 10 mice for MYC-PyMT + LP. Mice were sacrificed after 4-week LP diet treatment for immunofluorescence analysis. NP: control diet with 15% protein in weight (5CC7, TestDiet), LP: low protein diet with 2% protein in weight (5BT9, TestDiet). All statistical data are shown as mean ± S.D. Simple linear regression and GSEA based on the Kolmogorov Smirnov (K-S) test in (**a**), two-way ANOVA in (**b**), one-way ANOVA with the Tukey multiple comparison test correction in (**d**-**g**).

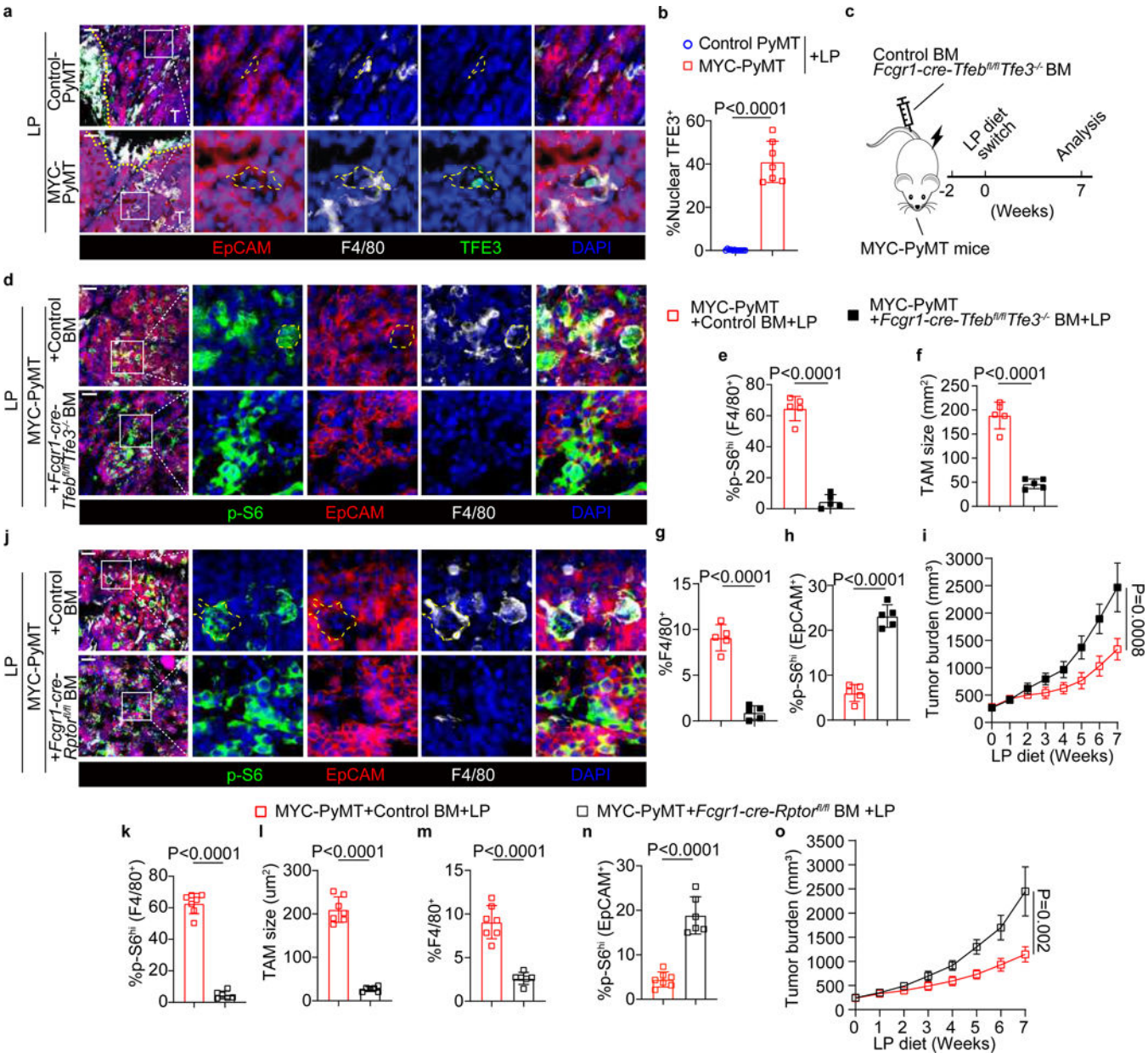

Fig. 3. TFEB/TFE3-dependent TAM mTORC1 activation suppresses cancer cell mTORC1 signaling.

a, Immunofluorescence images showing expression of EpCAM, F4/80, and TFE3 in 6 mm x 6 mm tumor tissue samples from mice of the indicated genotypes under a low protein (LP) diet condition (2% protein in weight, 5BT9, TestDiet). Scale bar: 50 μm. T: tumor parenchyma. Representative macrophages marked by yellow dashed lines. **b**, Quantification of percentage of cells with nuclear TFE3 among F4/80-expressing macrophages in the tumor parenchyma from control PyMT (n = 12) and MYC-PyMT (n = 7) mice. Tumor-bearing mice were sacrificed after 4-week LP diet treatment for immunofluorescence analysis. **c**, A schematic diagram showing dietary treatment of bone marrow (BM) chimera tumor-bearing mice. BM cells of control or *Fcgr1-cre-Tfeb*$^{fl/fl}$*Tfe3*$^{-/-}$ mice were transferred into

lethally irradiated MYC-PyMT mice with tumor burden around 250–350 mm^3, followed by switching to the LP diet two weeks after. **d**, **j**, Immunofluorescence images showing expression of phosphorylated S6 ribosomal protein at serine 240/244 (p-S6), EpCAM, and F4/80 in 6 mm x 6 mm tumor tissue samples in BM chimera mice of the indicated genotypes under the LP diet condition. Scale bar: 50 μm. Representative macrophages marked by yellow dashed lines. **e**, **k**, Quantification of percentage of cells with high p-S6 expression among F4/80-expressing macrophages in the tumor parenchyma. **f**, **l**, Quantification of cell size of F4/80-expressing macrophages. **g**, **m**, Quantification of percentage of F4/80-expressing macrophages. **h**, **n**, Quantification of percentage of cells with high p-S6 expression among EpCAM-expressing cancer cells. n = 5 mice for each group in (**e-h**); n = 7 mice for control BM, n = 6 mice for *Fcgr1-cre-Rptor*$^{fl/fl}$ BM in (**k-n**). Tumor-bearing mice were sacrificed after 4-week LP diet treatment for immunofluorescence analysis. **i**, **o**, Tumor burden in BM chimera mice of the indicated genotypes under the LP diet condition, including MYC-PyMT + control BM (n = 5) in (**i**), MYC-PyMT + *Fcgr1-cre-Tfeb*$^{fl/fl}$*Tfe3*$^{-/-}$ BM (n = 6) in (**i**), MYC-PyMT + control BM (n = 4) in (**o**) and MYC-PyMT + *Fcgr1-cre-Rptor*$^{fl/fl}$ BM (n = 5) in (**o**). All statistical data are shown as mean ± S.D. Two-sided Student t-test in (**b**, **e-h**, **k-n**) and two-way ANOVA in (**i**, **o**).

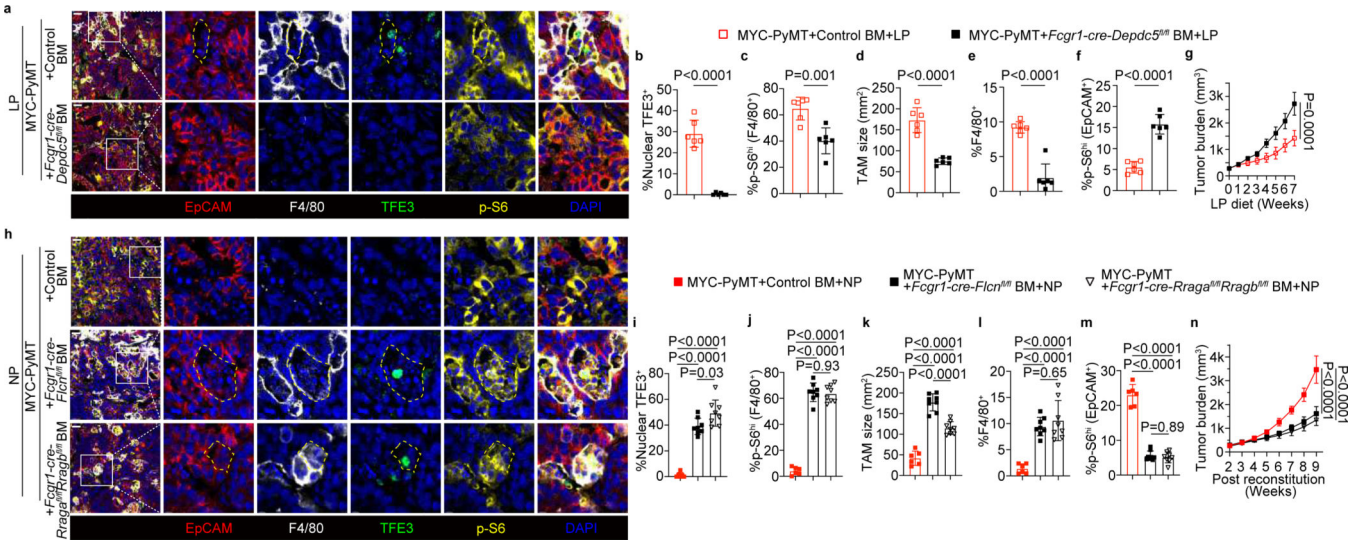

Fig. 4. The Rag GTPase nutrient-sensing pathway controls TFEB/TFE3-mTORC1 signaling in TAMs.

a, **h**, Immunofluorescence images showing expression of phosphorylated S6 ribosomal protein at serine 240/244 (p-S6), EpCAM, F4/80, and TFE3 in 6 mm x 6 mm tumor tissue samples in bone marrow (BM) chimera mice of the indicated genotypes under low protein (LP) diet (**a**) or normal protein (NP) diet (**h**) conditions. Scale bar: 20 μm. Representative macrophages marked by yellow dashed lines. **b**, **i**, Quantification of percentage of cells with nuclear TFE3 among F4/80-expressing macrophages in the tumor parenchyma. **c**, **j**, Quantification of percentage of cells with high p-S6 expression among F4/80-expressing macrophages. **d**, **k**, Quantification of cell size of F4/80-expressing macrophages. **e**, **l**, Quantification of percentage of F4/80-expressing macrophages. **f**, **m**, Quantification of percentage of cells with high p-S6 expression among EpCAM-expressing cancer cells. n = 6 mice for each group in (**b-f**), n = 6 mice for control BM in (**i-m**), n = 8 mice for both *Fcgr1-cre-Flcn*$^{fl/fl}$ BM and *Fcgr1-cre-Ragaa*$^{fl/fl}$*Ragb*$^{fl/fl}$ BM in (**i-m**). Tumor-bearing mice were sacrificed after 4-week LP diet treatment for immunofluorescence analysis. **g**, **n**, Tumor burden in BM chimera mice of the indicated genotypes under either the LP diet condition, including MYC-PyMT + control BM (n = 6) and MYC-PyMT + *Fcgr1-cre-Depdc5*$^{fl/fl}$ BM (n = 7), or the NP diet condition, including MYC-PyMT + control BM (n = 6), MYC-PyMT + *Fcgr1-cre-Flcn*$^{fl/fl}$ BM (n = 6) and MYC-PyMT + *Fcgr1-cre-Ragaa*$^{fl/fl}$*Ragb*$^{fl/fl}$ BM (n = 9). NP: control diet with 15% protein in weight (5CC7, TestDiet), LP: low protein diet with 2% protein in weight (5BT9, TestDiet). All statistical data are shown as mean ± S.D. Two-sided Student t-test in (**b-f**), two-way ANOVA in (**g**, **n**), and one-way ANOVA with the Tukey multiple comparison test correction in (**i-m**).

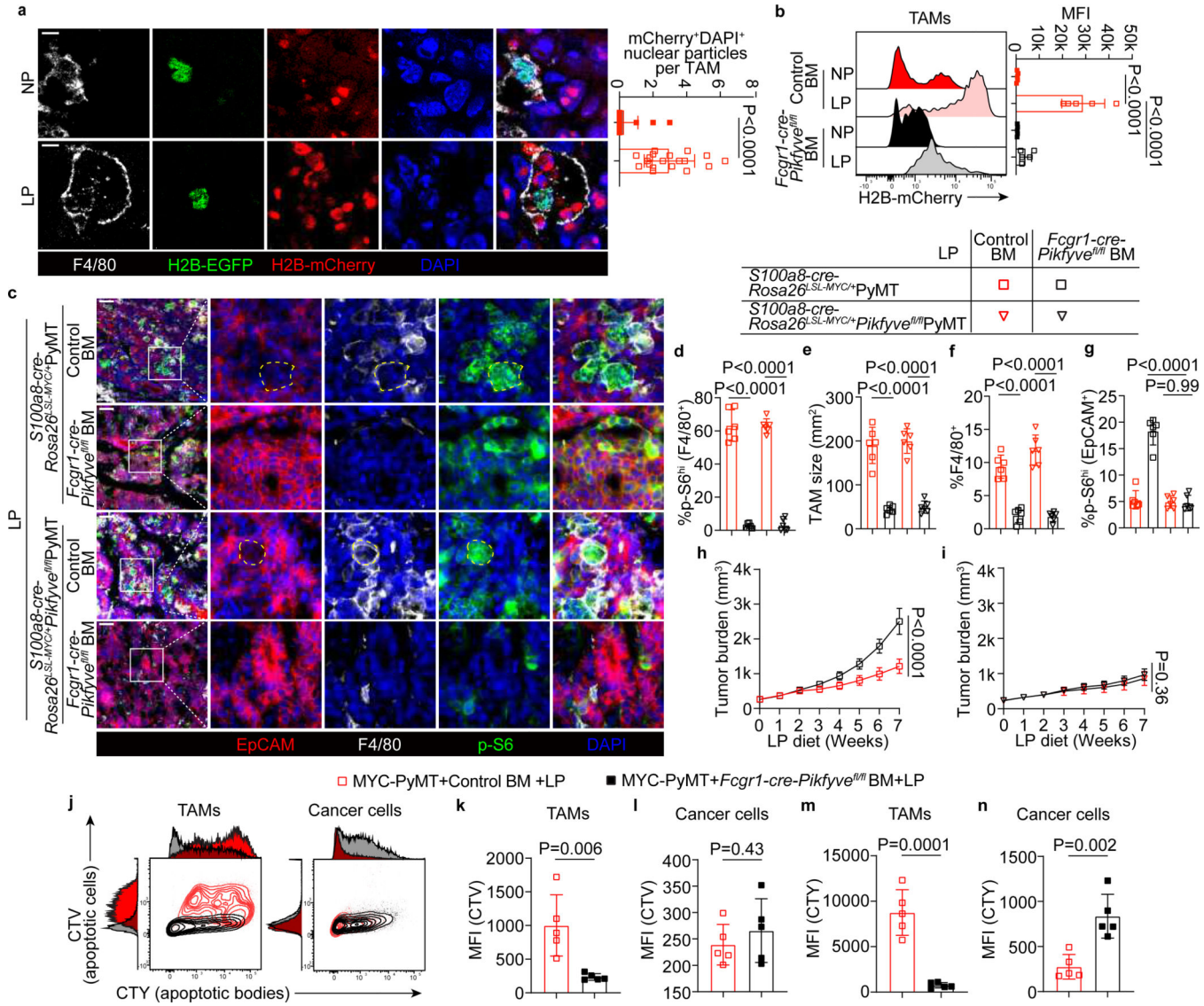

Fig. 5. Engulfment-mediated mTORC1 signaling dictates TAM and cancer cell competition.

a, Left panel: immunofluorescence images showing expression of F4/80, H2B-EGFP, and H2B-mCherry in 6 mm x 6 mm tumor tissue samples from bone marrow (BM) chimera mice made by transferring BM cells from *H2B-EGFP/H2B-EGFP* mice into lethally irradiated *S100a8-cre-Rosa26*$^{LSL\text{-}MYC/LSL\text{-}H2B\text{-}mCherry}$PyMT recipients under normal protein (NP) or low protein (LP) diet conditions. Scale bar: 5 μm. Right panel: quantification of mCherry and DAPI-double positive particles in F4/80-expressing macrophages under NP or LP diet conditions (n = 3 mice for each condition, data points are average numbers from each captured images). **b**, Flow cytometric analysis of engulfment of H2B-mCherry-positive apoptotic cancer cells by TAMs in BM chimera tumor-bearing *S100a8-cre-Rosa26*$^{LSL\text{-}MYC/LSL\text{-}H2B\text{-}mCherry}$PyMT mice with the indicated BM genotypes and NP or LP diet treatment conditions (left panel). Mean fluorescence intensity (MFI) of H2B-mCherry was quantified (right panel). n = 5 mice for each condition. **c**, Immunofluorescence images showing expression of phosphorylated S6 ribosomal protein at serine 240/244 (p-

S6), EpCAM, and F4/80 in 6 mm x 6 mm tumor tissue samples in BM chimera mice of the indicated genotypes under the LP diet condition. Scale bar: 50 μm. **d**, Quantification of percentage of cells with high p-S6 expression among F4/80-expressing macrophages in the tumor parenchyma. **e**, Quantification of cell size of F4/80-expressing macrophages. **f**, Quantification of percentage of F4/80-expressing macrophages. **g**, Quantification of percentage of cells with high p-S6 expression among EpCAM-expressing cancer cells. n = 6 mice for each group in (**d-g**). Tumor-bearing mice were sacrificed after 4-week LP diet treatment for immunofluorescence analysis. **h**, **i**, Tumor burden in BM chimera mice of the indicated genotypes under the LP diet condition [n = 6 in (**h**) and n = 8 in (**i**) for each group]. **j**. Flow cytometric analysis of engulfment of CellTrace Violet (CTV)- and CellTrace Yellow (CTY)-labeled apoptotic cells and apoptotic bodies by TAMs and cancer cells in control and *Fcgr1-cre-Pikfyve*$^{fl/fl}$ bone marrow chimeric MYC-PyMT mice under the LP diet condition. **k-n**. Quantification of CTV and CTY MFI signals in TAMs and cancer cells (n = 5 mice for each group). NP: control diet with 15% protein in weight (5CC7, TestDiet), LP: low protein diet with 2% protein in weight (5BT9, TestDiet). All statistical data are shown as mean ± S.D. Two-sided Student t-test in (**a, k-n**), one-way ANOVA with the Tukey multiple comparison test correction in (**b**, **d-g**), and two-way ANOVA in (**h**, **i**).